

## Democratizing EEG

### Embedding Electroencephalography in a Head-Mounted Display for Ubiquitous Brain-Computer Interfacing

Niforatos, Evangelos; He, Tianhao; Vourvopoulos, Athanasios; Giannakos, Michail

#### DOI

[10.1080/10447318.2024.2388368](https://doi.org/10.1080/10447318.2024.2388368)

#### Publication date

2024

#### Document Version

Final published version

#### Published in

International Journal of Human-Computer Interaction

#### Citation (APA)

Niforatos, E., He, T., Vourvopoulos, A., & Giannakos, M. (2024). Democratizing EEG: Embedding Electroencephalography in a Head-Mounted Display for Ubiquitous Brain-Computer Interfacing. *International Journal of Human-Computer Interaction*, 41 (2025)(11), 7015-7039. <https://doi.org/10.1080/10447318.2024.2388368>

#### Important note

To cite this publication, please use the final published version (if applicable). Please check the document version above.

#### Copyright

Other than for strictly personal use, it is not permitted to download, forward or distribute the text or part of it, without the consent of the author(s) and/or copyright holder(s), unless the work is under an open content license such as Creative Commons.

#### Takedown policy

Please contact us and provide details if you believe this document breaches copyrights. We will remove access to the work immediately and investigate your claim.



## Democratizing EEG: Embedding Electroencephalography in a Head-Mounted Display for Ubiquitous Brain-Computer Interfacing

Evangelos Niforatos, Tianhao He, Athanasios Vourvopoulos & Michail Giannakos

**To cite this article:** Evangelos Niforatos, Tianhao He, Athanasios Vourvopoulos & Michail Giannakos (19 Aug 2024): Democratizing EEG: Embedding Electroencephalography in a Head-Mounted Display for Ubiquitous Brain-Computer Interfacing, International Journal of Human-Computer Interaction, DOI: [10.1080/10447318.2024.2388368](https://doi.org/10.1080/10447318.2024.2388368)

**To link to this article:** <https://doi.org/10.1080/10447318.2024.2388368>



© 2024 The Author(s). Published with license by Taylor & Francis Group, LLC.



Published online: 19 Aug 2024.



Submit your article to this journal [↗](#)



Article views: 260




View related articles [↗](#)



View Crossmark data [↗](#)

# Democratizing EEG: Embedding Electroencephalography in a Head-Mounted Display for Ubiquitous Brain-Computer Interfacing

Evangelos Niforatos<sup>a</sup> , Tianhao He<sup>a</sup>, Athanasios Vourvopoulos<sup>b</sup>, and Michail Giannakos<sup>c</sup>

<sup>a</sup>Department of Sustainable Design Engineering, Delft University of Technology, Delft, Netherlands; <sup>b</sup>Bioengineering Department, Institute for Systems and Robotics (ISR-Lisboa), Instituto Superior Tecnico (IST), Universidade de Lisboa, Lisbon, Portugal; <sup>c</sup>Department of Computer Science, Norwegian University of Science and Technology, Trondheim, Norway

## ABSTRACT

Open hardware and the need for ecologically valid measurements drive the Electroencephalography (EEG) democratization movement—EEG has been steadily transcending the boundaries of clinical research, making its way into interdisciplinary fields. In Human-Computer Interaction (HCI), EEG is used to measure cognitive workload and infer cognitive processes for building cognition-aware systems. We describe and evaluate our *BCIglass* prototype where EEG electrodes are embedded in the frame of a mainstream Head-Mounted Display (HMD) to create a skull-peripheral topology. We devised a lab study with 34 participants who completed seven established cognitive tasks. Then, we conducted a pilot field study with one participant to test *BCIglass* in everyday-life settings. Our findings demonstrate that *BCIglass* captures EEG activity in a manner comparable to a research-grade EEG-cap system. Our topology infers the cognitive task at hand, and the underlying cognitive process(es) by proxy, with an accuracy of ~80% and only three electrodes at the skull periphery. Embedding EEG electrodes in lightweight HMDs represents a promising approach in the quest to achieve ubiquitous brain-computer interfacing in real-world settings.

## KEYWORDS

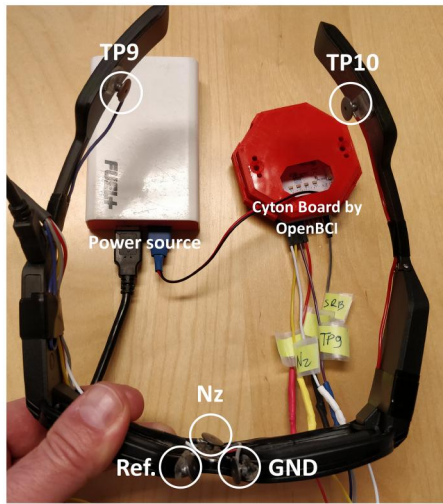
Electroencephalography; head-mounted displays; smart glasses; brain-computer interfaces; neuroergonomics

## 1. Introduction

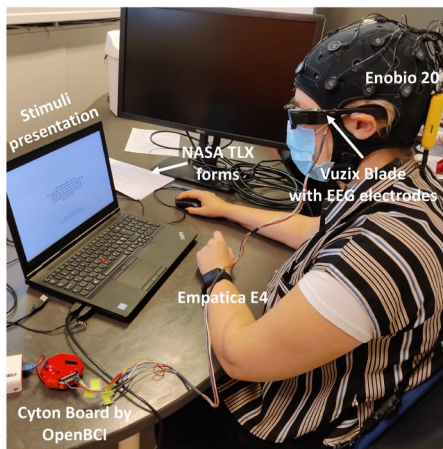
Electroencephalography (EEG) has been a fundamental diagnostic method in clinical neurology for almost a century, yielding numerous applications also in the field of HCI (Afergan et al., 2014; Cutrell & Tan, 2008; Fang et al., 2023; Ghiani et al., 2015; Grimes et al., 2008; Huang et al., 2014; Kar & Hazarika, 2023; Kosch et al., 2018; 2020; Lee et al., 2014; Mondellini et al., 2023; Nacke et al., 2011; Narsimha Reddy et al., 2023; Schneegass et al., 2020; Szafir & Mutlu, 2012; Vi & Subramanian, 2012). Originally, EEG was limited to confined clinical lab settings with sedentary subjects while adhering to strict clinical standards that often required bulky and niche equipment. EEG is highly susceptible to noise artifacts of external (e.g., electromagnetic interference from electronic devices and the power grid) and internal origins (e.g., physiological activity generated by muscle, eye, or cardiovascular signals). Inevitably, this sensitivity complicates the logistics of an EEG study, leading to lengthy and fatiguing sessions that often require Sisyphean patience from those participating, producing results with limited ecological validity. Gradually, EEG has become more pervasive, making its way into typical research labs by overcoming the necessity of following clinical policies. Hardware miniaturisation, lower cost, and improvements in noise reduction techniques, greatly increased the availability of EEG. In the past

~15 years, there have been initiatives to make EEG more ubiquitous by moving it out of the lab and into everyday life. These initiatives are driven by the need to obtain more naturalistic EEG measurements, such as when at work or at home, and have been supported by the grassroots movements of open hardware and “Do-It-Yourself” (DIY) (e.g., OpenBCI).<sup>1</sup> Exemplary approaches attempt to move EEG in the wild by concealing it in a baseball cap (Lin et al., 2008) or behind the ear as an eartube (Bleichner & Debener, 2017). Advancements in the field of EEG signal processing enable the real-time removal of noise artifacts generated by muscle contractions and body movement such as facial expressions, speech, walking or even jumping<sup>2</sup> (see “Artifacts Subspace Reconstruction” algorithm (Kumaravel et al., 2021; Mullen et al., 2015; Tsai et al., 2022)). In this paper, we propose and evaluate a sparse EEG electrode topology embedded in the form factor of a modern Head-Mounted Display, as a medium for moving EEG outside the lab and into the users’ everyday-life settings. We deem this is the necessary step before activating the HMD to incorporate relevant input (e.g., Augmented Reality—AR overlays), effectively creating a “closed-loop” system (Figure 1).

Head-Mounted Displays (HMDs), or “smart glasses,” bear an unprecedented potential to alter the way we produce and consume information, revolutionizing our everyday

(a) The *BCIGlass* prototype.

(b) A user wearing our prototype.



(c) A participant with both systems.

**Figure 1.** We evaluated our *BCIGlass* prototype (5 electrodes) by comparing it to the research-grade Enobio 20 system (20 electrodes) in a lab study with 34 participants.

lives. Either reading the latest news headlines, revisiting our grocery list, or seeking information online and navigating when on the go (Rehman & Cao, 2016), a great number of daily tasks can be revamped by the unique form factor of

HMDs. Situated in front of our eyes and around our skull, HMDs are directly interposed between what we can see and hear, thus influencing our perceptual and cognitive capacities. HMDs bear significant benefits for augmenting our cognitive capacities, such as enhancing procedural learning (Tang et al., 2003), improving spatial cognition for the elderly (Kim & Dey, 2009), and supporting decision-making in challenging environments (Fedosov et al., 2016). In fact, EEG has been utilized for mitigating HMD implications, such as for estimating visual discomfort (Mai et al., 2017). In this work, we merge EEG and HMDs to pave the way for cognition-aware systems (Dingler & Niforatos, 2021) by producing the following contributions:

- We introduce a sparse *BCIGlass* prototype with a concealed EEG-electrode topology embedded in the frames of a modern and lightweight HMD.
- We used a total of seven (7) cognitive tasks able to induce a wide spectrum of cognitive processes and cognitive workload reflected in objective, subjective, and physiological measures.
- We showcase how our *BCIGlass* prototype can implicitly infer the cognitive processes involved in seven different cognitive tasks.
- We demonstrate how our *BCIGlass* prototype captures EEG activity in a similar manner to a higher-resolution EEG system by utilizing the compound EEG measure of Engagement Index.
- We train a set of classifiers that predict the type (class) of the cognitive task at hand with an improved accuracy-over-electrode ratio for our *BCIGlass* prototype.
- We share early findings from a pilot deployment of the *BCIGlass* prototype with one participant in the wild.

## 2. Background

The idea of embedding EEG in headwear and eyewear is not new. Lin et al. introduced a Brain-Computer Interface (BCI) prototype that encases a wireless EEG device in a typical baseball hat (Lin et al., 2008). The motivation was to develop a BCI system that monitors the physiological state of drivers in real time to detect and warn about increasing drowsiness levels. Bleichner and Debener, motivated by EEG signal acquisition in natural daily-life settings, introduced a flex-printed sensor array equipped with EEG electrodes that is worn around the human ear (Bleichner & Debener, 2017). The authors showcased how their ear-EEG prototype was able to record meaningful continuous EEG signals, ERPs and neural oscillations. In-ear EEG approaches (e.g., (Kaveh et al., 2020)) have also proliferated for measuring alpha band fluctuations during speech (Ala et al., 2022), measuring sleep quality (Henao et al., 2022), and detecting epileptic discharges in patients suffering from Alzheimer’s disease (Musaeus et al., 2023). A recent study assessed focus by comparing between conventional cap-based EEG and mobile in-and around-the ear EEG systems (Cr  tot-Richert et al., 2023). However, ear-EEG approaches are by default limited to a location in-and around-the ear, with a low number of



electrodes which in turn reduce the quality and the signal types they can detect and the applications they can support (Kaongoen et al., 2023).

### 2.1. EEG in eyewear and head-mounted displays

Kim et al. introduced an experimental hybrid-BCI smart glasses prototype with protruding EEG electrodes, which also utilizes eye-tracking, to remotely control domestic appliances (Kim et al., 2015). By capturing event-related potentials and eye-gaze patterns, they were able to achieve an overall average accuracy of 70.83% in remotely controlling a TV. Various commercial eyewear products claim to utilize EEG (or EOG—electrooculography) at the contact points with the skull to provide so-called “neurofeedback.” For example, Narbis sunglasses<sup>3</sup> utilize three electrodes, two at the back of the temples of the device touching the left and right mastoids, and one at the tip of a protruding arm that touches the top of the skull, for tracking concentration. When concentration is low, the Narbis electrochromic lenses start darkening for inviting the user to focus more. Lowdown Focus by Smith,<sup>4</sup> and powered by MUSE, employs a more socially acceptable design equipping a plastic pair of sunglasses with silicon electrodes at the edges of the temples that touch the left and right mastoid processes (Krigolson et al., 2017). A companion mobile application connects to the Lowdown Focus sunglasses for collecting the readings to track and increase one’s concentration levels. JINS MEME<sup>5</sup> is perhaps the most prominent eyewear that employs near-skull contact for providing neurofeedback. JINS MEME utilizes two electrodes embedded in the bridge of the eyewear that touches the nasal bone to detect concentration levels by measuring the duration and the number of eye blinks via EOG (Uema & Inoue, 2017).

### 2.2. Applications

The combination of eyewear with EEG yields promising niche applications in the intersection of HCI and Ubiquitous Computing with several domains such as health-care, learning, and lifestyle (Chwalek et al., 2021). e-Glass is an EEG-enabled eyewear that employs an OpenBCI board and a set of electrodes across the inner side of the frame for detecting epileptic seizures (Sopic et al., 2018). The PhysioHMD prototype adopts a bulky “mask” design that occludes part of the face for hosting a wide range of physiological sensors, including EEG electrodes, capturing also facial expressions (Bernal et al., 2018). Several Virtual Reality (VR) headsets utilize their extensive contact with the skull to embed among other sensors also EEG electrodes for measuring brain activity (e.g., LUCY<sup>6</sup> and Neurable<sup>7</sup> (Jantz et al., 2017)). In recent years, the combination of EEG with HMDs has been mostly driven by the field Augmented Reality (AR). A systematic literature review on wearable EEG devices reports a limited number of instances where EEG electrodes are actually embedded in eyewear and lightweight HMD frames (Kaongoen et al., 2023). Instead, EEG has been extensively combined with AR headsets mainly in the form of an EEG cap (Angrisani et al., 2023; Arpaia

et al., 2022; Jang et al., 2023; Zhao et al., 2020). Typically, EEG and HMD combination aims to enhance user experience and utility by providing real-time brain activity feedback, driving more immersive and adaptive environments, or powering specialized applications. For example, an EEG cap has been combined with the HoloLens 2<sup>8</sup> AR headset to investigate Steady-State Visual Evoked Potentials (SSVEP) in AR to support smart home, ambient assisted living, gaming and other applications (Zhao et al., 2020). Similarly, Arpaia et al. benchmark three different AR headsets (Epson Moverio, Oculus Rift, and HoloLens 2) in their ability to induce SSVEPs captured via an EEG cap (Arpaia et al., 2022). The combination of EEG caps and AR headsets has also been explored for authentication purposes. Jang et al. effectively combine HoloLens 2 with an EEG cap to deliver rapid serial visual presentation (RSVP) of images and capture the evoked Event-Related Potentials (ERPs), respectively (Jang et al., 2023). A recent literature review by Angrisani et al. highlights the increasing trend of combining EEG caps with AR for SSVEP and similar applications (Angrisani et al., 2023). However, due to their bulk and lack of EEG-electrode integration in the HMD frame, all these approaches are limited to indoor settings, while they suffer from low social acceptability.

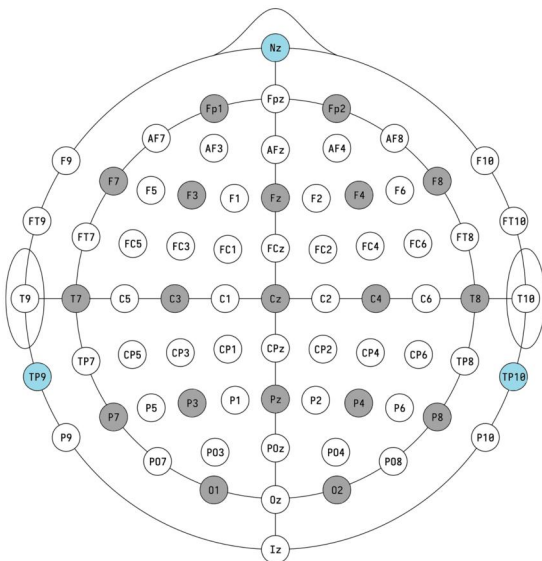
In the context of this work, we use the term “social acceptability” to refer to a combination of factors that would encourage (or discourage) a user to wear and interact with an HMD in public (Koelle et al., 2015). Factors that influence social acceptability are societal norms and perception, user comfort and ergonomics, context of use, culture, and impact on social interaction (Koelle et al., 2015). For an overview of the challenges hindering the adoption and use of HMDs in public, see (Gugenheimer et al., 2019). Despite the fact that we do not measure social acceptability directly, our assumption is that a slimmer HMD form factor (e.g., eyewear), concealing embedded EEG electrodes, is by default more socially acceptable than a full face HMD or AR headset (e.g., HoloLens 2) and/or an EEG cap. To avoid confusion, we resort to using the term “lightweight” to describe HMDs with high social acceptability potential. The EEGlass prototype conceals five EEG electrodes in a typical frame of a pair of glasses at its touchpoints with the skull (Vourvopoulos et al., 2019). The authors showed that a skull-peripheral EEG topology was able to capture brain activity related to resting-state but also motor preparation and execution. However, the trials included only one participant with no cognitive measures, no task-performance baseline, and no cognitive-state inference.

Here, we build on the work of Vourvopoulos et al. and introduce a prototype merger (*BCIglass*) between a modern HMD (Vuzix Blade) and an open-source EEG platform (OpenBCI). We then investigate how effectively the *BCIglass* prototype can capture EEG activity, infer cognitive processes, and predict the cognitive task at hand, by comparing it with a high-resolution EEG-cap system (Enobio 20) in a lab study with 34 participants. Finally, we test the *BCIglass* prototype in real-life settings with one participant.

### 3. BCIGlass

Our prototype is a merger between the Vuzix Blade<sup>9</sup> HMD and the 8-channel Cyton<sup>10</sup> biosensing board by OpenBCI (250 Hz sampling rate). OpenBCI is a popular and affordable open hardware and software platform for the collection and analysis of biosignals (e.g., EEG, heart rate, etc.), inspired by the grassroots movement of DIY (Vourvopoulos & Bermudez I Badia, 2016). The Cyton board is equipped with 8 biopotential input channels (for hosting up to 8 electrodes), a 3-axis accelerometer, local storage, and wireless communication modules. No additional electronic components are used. Evidently, our prototype electrode topology is imposed by the HMD's form factor and limited to its contact points with the skull. Thus, our HMD topology utilizes three flat Ag/AgCl electrodes (plus two for reference and ground) based on the 10-10 system (see Figure 2(a)) for measuring EEG activity: one electrode placed inwards above the HMD bridge touching the skull at the glabella (between the eyebrows), and two electrodes at the inner-back side of the HMD temples, touching the left and right mastoid processes, behind the left and right ear, respectively (see Figure 1(a)). Commercial EEG devices, such as the Mindwave Neurosky, have shown that a single electrode placed over the frontal lobe area (Fpz) is able to inform a BCI in controlling the speed of a robot (Katona et al., 2016). Due to the HMD form factor, the Nz electrode is placed by default lower than the Fpz electrode location. However, due to volume conduction over the scalp, we expect we will be able to capture sufficient EEG activity from the Nz electrode too. The reference and ground electrodes are placed at the inner part of the HMD bridge, touching the left and right sides of the nasal bone, respectively. The reasons we opted for the Vuzix Blade HMD are:

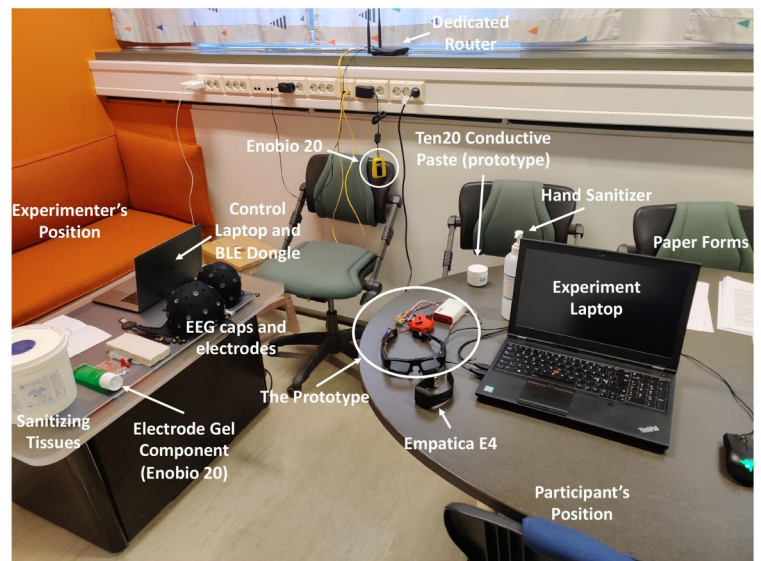
1. *Form factor.* The temples (aka. "arms") are slightly curved inwards to secure a stable grip around the skull. This ensures continuous contact between the electrodes and the skull even when motion is involved.



(a) Our experimental *BCIGlass* electrode topology in light blue vs. the baseline Enobio 20 electrode topology in grey (10-10 system).

2. *Lightweight.* Good balance between a lightweight frame design (90 g) with increased social acceptability and available space for embedding the EEG electrodes.
3. *Display and tinted lenses.* Good display visibility renders the perception of stimuli presented on the display more probable, thus being instrumental in designing a closed-loop system in the future. In this study, the Vuzix Blade HMD was deactivated and no AR stimuli were projected.
4. *Operating system.* Android OS enables quick prototyping and deployment of experimental mobile/wearable applications.
5. *On-board camera and sensors.* Equipped with a front-facing camera (1080p), integrated speakers, and additional sensors (e.g., inertia measurement unit) for activity recognition.
6. *Connectivity.* Bluetooth and Wi-Fi connectivity.
7. *Electromagnetic compatibility (EMC).* Vuzix devices have been systematically tested to ensure that they emit little to no electromagnetic field. Thus, they are eligible for use in healthcare and medical settings (see IEC 60601-1-2:2014 international standard).<sup>11</sup>

However, due to the close proximity of the OpenBCI electrodes to the internal Vuzix Blade circuitry, and its potential to influence the EEG signal, we deemed purposeful to investigate the electromagnetic fingerprint of the Vuzix Blade HMD. To this end, we used the GQ EMF-390<sup>12</sup> electromagnetic field (EMF), electrical field (EF) and Radio Frequency Field (RFF) meter to measure the EMF generated by an active Vuzix Blade in very close proximity. The GQ EMF-390 is equipped with a 3-axis EMF sensor (0.5 Hz–150KHz), an EF sensor (0–1000 V/m) and an RFF sensor (10 MHz–10 GHz). First, we used the EMF meter to find a location with relatively low ambient EMF and establish a baseline. Then, with the Vuzix Blade powered on, we used



(b) The experimental apparatus and the lab setup.

**Figure 2.** EEG electrode topologies for both systems and experimental apparatus.



the GQ EMF-390 to measure EMF, RF and RFF from the inner side of the frame and at the locations of all *BCIglass* electrodes. With the exception of the TP9, which displayed high periodic RFF, no other electrode displayed notable EMF, EF and RFF measurements (see Figure 3(a)). A closer inspection of the RFF time series shows periodic peaks resembling a connectivity signal pattern with a max. peak of  $382 \text{ mW/m}^2$ . Indeed, the GQ EMF-390 meter classifies the RF activity as “Wi-Fi/Phone” (see Figure 3(a)). A synchronous RF power spectrum analysis showcases that Vuzix Blade periodically emits in the 2.4 GHz band reserved for Wi-Fi connectivity (see Figure 3(b)). Even so, the usable EEG frequency spectrum spans between 1 and 100 Hz, and thus *BCIglass* EEG measurements should not be affected by Wi-Fi connectivity. Ultimately, our aim with the *BCIglass* prototype is to deliver a closed-loop EEG/BCI platform that is lightweight, robust to motion, unobtrusive, and socially acceptable, thus suitable for use in everyday-life settings. Here, we investigate the effectiveness of our prototype in lab settings and we make the first step towards introducing it into the wild.

#### 4. Materials and methods

Initially, we evaluated the effectiveness of our *BCIglass* prototype in stationary lab settings, by comparing it against a system with a dense electrode topology (Enobio 20). We pose the following Research Questions (RQs) as a first important step towards introducing EEG into the wild by merging it with HMDs:

**RQ1. How effective are the employed cognitive tasks in inducing a wide spectrum of cognitive workload?**

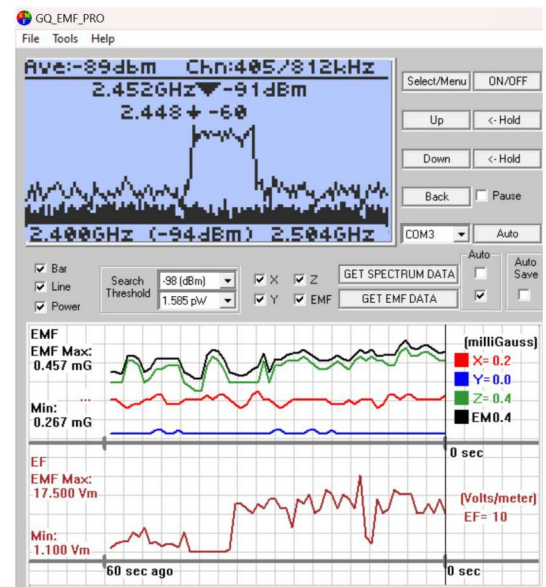
This is an internal validity RQ: We employ a total of seven (7) cognitive tasks based on cognitive interventions commonly performed in the fields of psychology, cognitive science, and neuroscience (see Section 4.3). To confirm how challenging these tasks will be for our participants, we devised a series of objective and subjective measures that characterise cognitive performance (e.g., scores, completion times) and subjective workload (e.g., NASA TLX (Hart & Staveland, 1988)). We also utilized physiological measures, such as electrodermal activity (EDA) and skin temperature (ST) as additional indicators of stress and cognitive workload (Abdelrahman et al., 2017; Setz et al., 2009). We expect that the diversity of the cognitive tasks that we employ will require different levels of cognitive processing (multiple cognitive processes), resulting in systematic variations in cognitive performance and cognitive workload. In turn, this will be reflected in participants’ objective, subjective and physiological measures across the cognitive tasks.

**RQ2. Can the *BCIglass* electrode topology capture and infer the cognitive processes elicited during cognitive tasks?**

The diversity of the employed cognitive tasks will result in invoking a variety of cognitive processes that in turn produce different relative EEG band power (Başar et al., 2001; Buzsáki & Draguhn, 2004). Thus, by detecting and measuring the EEG band power, we can roughly estimate the type of the underlying cognitive process(es). First, we expect that our *BCIglass* electrode topology will be able to capture reductions in Alpha relative band power as an indicator of cognitive workload in



(a) Only the TP9 electrode location displayed high RFF periodically (max.  $382 \text{ mW/m}^2$ ) hinting at an internal Wi-Fi antenna as indicated by the GQ EMF-390 meter.



(b) An RF spectrum power analysis shows that Vuzix Blade HMD periodically emits in the  $\sim 2.4\text{--}2.5$  GHz band, far above the usable EEG frequency spectrum (1–100 Hz).

**Figure 3.** We used the GQ EMF-390 meter to measure Electromagnetic Field (EMF in 0–500 mG at 0.5 Hz–150 KHz), Electrical Field (EF in 0–1000 V/m) and Radio Frequency Field (RFF in  $\text{mW/m}^2$  at 10 MHz–10 GHz), generated by an active Vuzix Blade HMD, across the *BCIglass* electrode topology. Our results indicate that the *BCIglass* EEG signal quality should remain unaffected by the operation of the Vuzix Blade HMD.

cognitively demanding tasks, when comparing it to a baseline (Klimesch et al., 1993). Working memory function is related with Theta and Alpha band-power fluctuations (Klimesch, 1999), which we expect to capture during high memory workloads (Mecklinger et al., 1992). Decision-making is reflected by the Theta band, especially in oddball paradigms during willed attention tasks (Rajan et al., 2019), and it is known to increase linearly with increasing interference between incongruent stimuli (Hanslmayr et al., 2008). In contrast, we do not expect that our *BCIglass* topology will capture significant differences across tasks for the Beta band, since it is more frequently associated with motor preparation and execution (Crone et al., 1998). However, we expect that Delta band-power fluctuations will be more pervasive throughout most cognitive tasks, since the Delta band characterizes increased attention to internal processing during mental tasks (Harmony et al., 1996).

**RQ3. How does the *BCIglass* electrode topology compare against a higher-resolution EEG-cap topology in capturing EEG activity and classifying the cognitive task at hand?**

Our expectation is that our *BCIglass* electrode topology will capture EEG activity in a similar fashion to the Enobio 20 topology due to the propagation of EEG signals over the scalp. In other words, even with fewer electrodes situated only at the periphery of the skull, the EEG activity captured by our prototype will not differ substantially from that captured by a higher-resolution EEG device (Enobio 20). As additional evidence, we expect that both topologies will result in composite brain-activity measures, such as the Engagement Index, that will display significant correlations with subjective workload measures (e.g., NASA TLX) (Kamzanova et al., 2014; Pope et al., 1995). Finally, we expect that the *BCIglass* topology will capture EEG activity in sufficient quality to enable the prediction of the type of cognitive task at hand as a proxy of the underlying cognitive process(es) when using prominent classification algorithms for BCIs (Lotte et al., 2018).

#### 4.1. Participants

We recruited a total of 34 healthy and right-handed participants (17 female and 17 male) from the premises of our University with no history of neurological disorders, and an average age of 30.18 years ( $SD = 4.528$ ). Most of our participants were University employees ( $N = 25$ ) such as doctoral candidates, postdocs and professors, followed by University undergraduates ( $N = 7$ ), and private employees ( $N = 2$ ). Participants with vision acuity below 20/20 were asked beforehand to wear prescription contact lenses during the trials. All participants provided their informed consent after which the trials commenced. At the end of the study, participants were debriefed and compensated for their time with a cinema ticket card of 20 credits.

#### 4.2. Apparatus

Our experimental setup (see Figure 2(b)) was optimized for comparing between two EEG systems/topologies: Our *BCIglass* prototype as the experimental system and the Enobio 20<sup>13</sup> (Neuroelectronics, Barcelona, Spain | 20 Ag/AgCl gel electrodes

at 500 Hz sampling rate) as the baseline system, for comparing between the two distinct electrode topologies (see Figure 2(a)). We used two laptop computers, (1) an “experiment laptop” and (2) a “control laptop.” The experiment laptop was connected to a USB mouse for collecting participants’ responses in the form of right & left mouse clicks. The experiment laptop ran a custom Presentation<sup>14</sup> stimulus software and the Neuroelectronics Instrument Controller (NIC) software for collecting the EEG data from the Enobio 20 (via USB). The control laptop collected the EEG data from the *BCIglass* prototype (via a BLE dongle) running the “OpenBCI\_GUI” application. A dedicated Wi-Fi router was used to create a local area network where both laptops could connect and transmit data with minimum latency. Using the aforementioned software, both laptops transmitted EEG data over the same network by utilizing the Lab Streaming Layer<sup>15</sup> (LSL) transmission control protocol. The control laptop was also running the LSL “Lab Recorder” software for collecting, syncing, and storing the data streams from the *BCIglass* prototype, the Enobio 20, and the “Presentation” software (event markers). We also used the Empatica E4 physiological wristband to collect physiological data such as Heart Rate (HR), Electrodermal Activity (EDA), and skin temperature (ST), along with 3-axes acceleration measurements.

#### 4.3. Cognitive tasks and baselines

In total, we devised seven (7) cognitive tasks grouped in three classes: (a) one 2-back task, (b) two Backward Masking tasks, and (c) four Stroop tasks (see Figure 4 and Table 1). The purpose of the cognitive tasks was the elicitation of cognitive processes, related to working memory, (willed) attention, conscious/unconscious processing, and cognitive workload, in an attempt to investigate how these can be captured by our *BCIglass* prototype in comparison to a higher-resolution EEG system (Enobio 20). All cognitive tasks were delivered via the “Presentation” (Neurobehavioral Systems, CA, USA) software, a stimulus delivery and experiment control program for neuroscience. We also recorded resting-state brain activity for the period of 4 minutes during “eyes open” and “eyes closed” (2 min each). For an overview of the cognitive tasks, see Figure 4 and Table 1.

#### 4.4. Procedure

##### 4.4.1. Preparation

Participants arrived individually to the lab where we informed them about the purpose of our experiment. Next, they took their dedicated spot in front of the experiment laptop (see Figure 2(b)), provided their informed consent, and completed the demographics questionnaire. After measuring their skull circumference, we fixated a fitting EEG cap on participants’ heads, and helped them to wear the *BCIglass* prototype as a typical pair of glasses. We applied electrode gel component and ten20 conductive paste to Enobio 20 and the *BCIglass* electrodes, respectively. We connected the Enobio 20 via USB to the experiment laptop, and tested electrode impedance with the NIC software. We



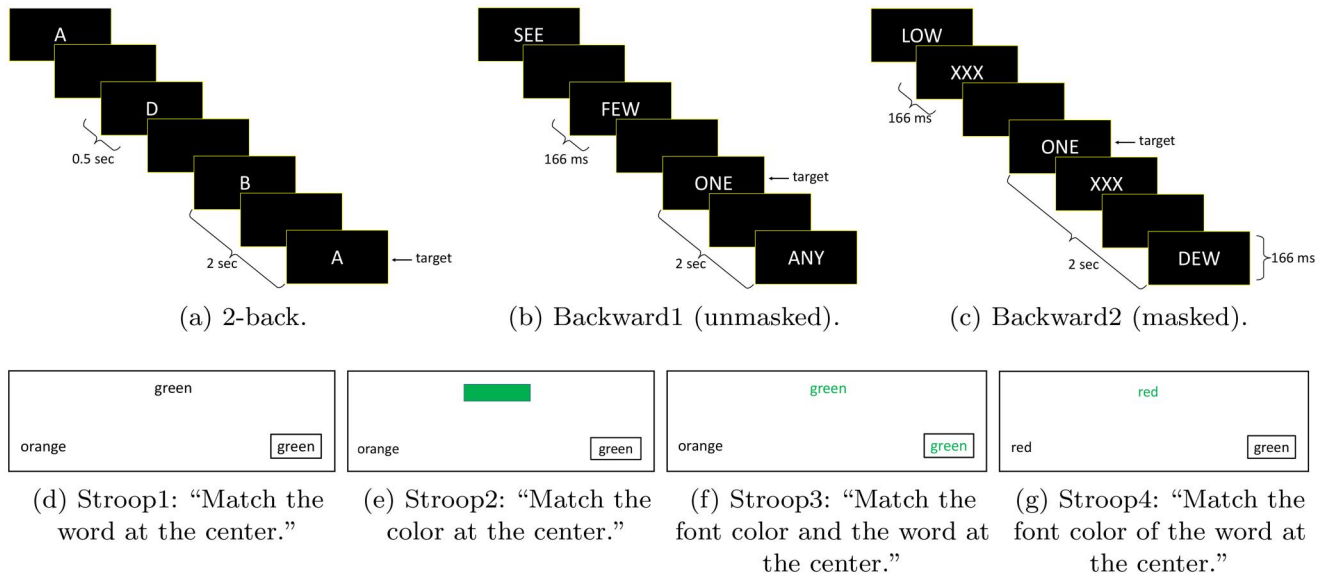


**Figure 4.** All seven (7) cognitive tasks used in our experiment. The n-back task has been employed in literature as a working-memory test (Jaeggi et al., 2010; Kane et al., 2007). The Backward masking task is a visual task with a visual stimulus presented to a subject only to be immediately followed by another visual “stimulus” that masks the previous stimulus. Backward-masking tasks are used to quantify the amount of time that information takes to pass through the sensory memory and serve as a measure of cognitive-processing efficiency (Verney et al., 2004). The Stroop task involves the presentation of a colour word (e.g., “red”) but in incongruent font colour (e.g., green). During a Stroop task, time–frequency analyses have shown that theta oscillations increased linearly with increasing stimulus interference (incongruence) (Hanslmayr et al., 2008).

**Table 1.** Average scores and response times for all cognitive tasks followed by Standard Deviations (SD) in parentheses.

Cognitive task	Class	Fig.	Trials (N)	Task progression	Performance score (%)	Subjective workload (%)	Response time (ms)
2-back	1	4(a)	22	Time	75.882 (20.760)	48.926 (16.772)	721.834 (222.643)
Backward1	2	4(b)	32	Time	99.019 (3.980)	30.345 (12.992)	403.576 (59.149)
Backward2	2	4(c)	32	Time	69.607 (33.951)	58.146 (16.910)	669.672 (349.912)
Stroop1	3	4(d)	20	Participant	99.558 (1.894)	20.424 (11.396)	834.322 (169.943)
Stroop2	3	4(e)	20	Participant	99.411 (2.046)	23.319 (12.726)	979.435 (144.246)
Stroop3	3	4(f)	20	Participant	99.852 (.857)	23.132 (15.578)	981.566 (270.916)
Stroop4	3	4(g)	20	Participant	91.911 (11.282)	36.904 (16.874)	1648.295 (442.673)

connected the *BCIglass* prototype via the BLE dongle to the control laptop, and tested electrode impedance with the OpenBCI\_GUI app. For both systems, electrode impedance was maintained below 20 k $\Omega$  by applying additional electrode gel component and conductive paste when required. Participants also wore the Empatica E4 physiological wristband on their left wrist. This study was approved by the Norwegian Centre for Research Data (NSD/ref. nr.: 963870).

#### 4.4.2. Training and main session

For each participant, we devised a different experimental plan following the Latin square counterbalancing technique for cancelling out sequential (carry-over) effects (Bradley, 1958). This ensured that all combinations of cognitive task classes occurred in a certain order and for an equal number of times. We only counterbalanced between the three task classes and not within (see Table 1), since the Backward masking and Stroop task classes were designed for gradually increasing difficulty. First, we offered our participants a training session where they completed all the cognitive tests in the order of their experimental plan. All cognitive tasks could be completed by left and/or right mouse clicks. After the training session was over, the actual study commenced. The EEG acquisition stage began with a 4-minute period for

acquiring resting state data. The resting state data was acquired during two 2-minute periods with eyes open and eyes closed, respectively. We instructed our participants to remain silent while either fixating their eye-gaze on a black cross displayed on the screen, or when having their eyes closed. During the actual session, the participants repeated the same tasks they had performed in the training session and in the same order (see Figure 1(c)). The main session differed only in that participants were asked to fill in a NASA-TLX form after the completion of each cognitive task (seven in total). In the NASA-TLX forms, participants reported on their subjective workload in the tasks they had just completed. The main session concluded when all seven (7) tasks and NASA TLX forms were completed.

#### 4.4.3. Post-session

After all equipment was carefully removed, participants were debriefed about their experience regarding the mounted equipment (*BCIglass* and Enobio 20), the cognitive tasks they had completed, and any insight they would like to share. We thanked our participants and we provided them with the compensation. The trials took place in October–November 2020 and during the COVID-19 pandemic. We followed all hygiene regulations by sanitizing our wearable equipment and the lab

space after each session (Simmons & Luck, 2020). Participants were also asked to wear masks during the experiment, following our University's policy for COVID-19.

#### 4.5. EEG data analysis

All EEG signals were processed in MATLAB® (The MathWorks, Natick, MA) with the EEGLAB toolbox (Delorme & Makeig, 2004). After importing the data together with the channel info, a high-pass filter at 1 Hz was used to remove the “baseline drift,” followed by line-noise and harmonics removal at 50 Hz. Furthermore, bad channels were rejected, and the data was subsequently re-referenced to average to achieve high signal-to-noise ratio (SNR). Any potential missing channels had been interpolated to minimize a potential bias in the re-referencing stage. Next, an Independent Component Analysis (ICA) was performed for removing eye blinking, and movement artifacts (Makeig et al., 1996). For the independent components (IC) labeling, we performed manual artifact recognition by inspecting the different components both in the time and frequency domain, and also by using the ICLabel plugin from EEGLAB. The ICLabel plugin includes a trained classifier for EEG independent component analysis which examines the probability of a component falling in the seven categories: brain, muscle, eye, heart, line noise, channel noise, and other. The ICLabel classifier is trained by using crowd-sourced data labeling or crowd labeling (Pion-Tonachini et al., 2017). Data-epoching was performed for eyes-open vs. eyes-closed baselines, followed by time/frequency decomposition between 1–30 Hz with a 3-cycle wavelet (a Hanning-tapered window was applied (Kabe & Sako, 2020)). For extracting the EEG bands, the Welch's method for Power Spectral Density (PSD) of the power spectrum was used (Welch, 1967). This included

the average relative spectral power ( $\mu V^2/Hz$ ) across the following frequency bands during the cognitive tasks: Delta (1–4 Hz), Theta (4–7 Hz), Alpha (8–12 Hz), and Beta (12–30 Hz) over the total power. In addition, PSD from resting-state Alpha was computed during eyes-open and eyes-closed sessions before the trials (see Figure 7). We also calculated the Engagement Index (EI) across all cognitive tasks, for all three electrodes of our prototype, and the Cz and Pz electrodes of Enobio 20, respectively. The EI is computed as  $EI = Beta / (Alpha + Theta)$  and is known for correlating with participants' self-reported task engagement (Kamzanova et al., 2014; Pope et al., 1995). Finally, we used custom Python scripts to synchronize physiological input recorded by Empatica E4 with the EEG data and for producing aggregates and simple features (e.g., means and peaks).

#### 5. Statistical analyses and results

We performed all the necessary pre-tests, such as Shapiro-Wilk tests of normality, Levene's tests of homogeneity of variance, and Mauchly's tests of sphericity before carrying out typical inferential statistical tests (e.g., Analysis of Variance, *t*-tests, etc.). We omit the pre-tests for the sake of brevity. Unless specified otherwise, the null hypothesis ( $H_0$ )

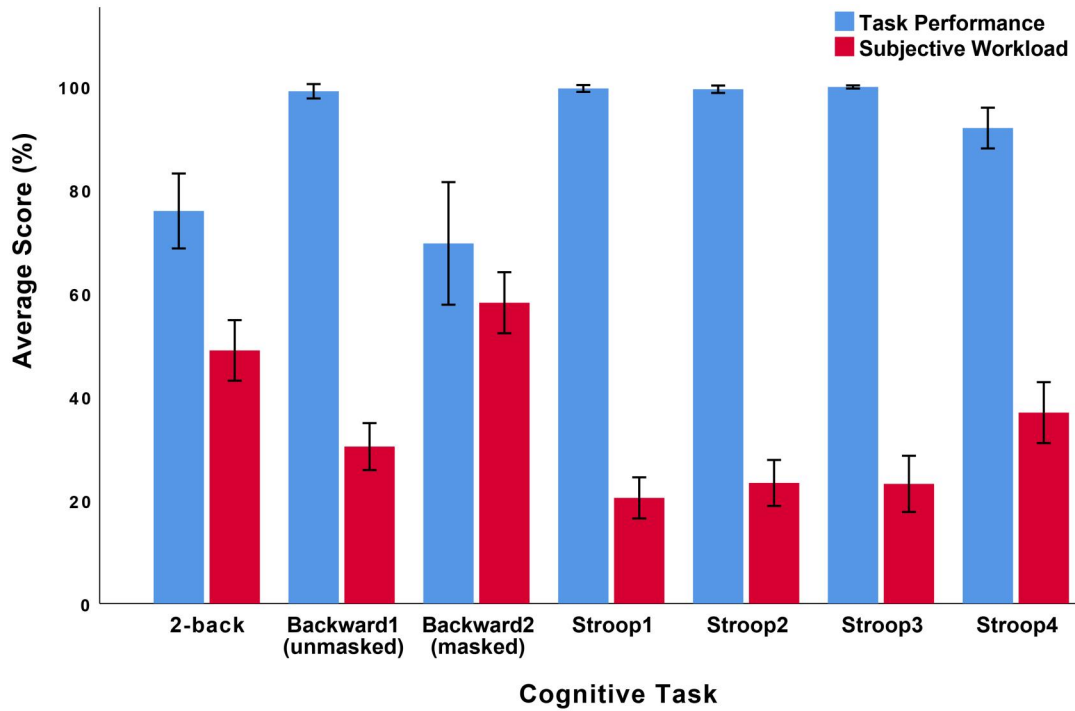
of the statistical tests performed here assumes no significant differences observed, and the *p*-value was adjusted to .05 to control for Type I error rate. Post-hoc pairwise tests for multiple comparisons apply the Bonferroni correction against Type I errors. Depending on the statistical test at hand, we report averages and standard deviations (parametric) or median values (non-parametric).

##### 5.1. Cognitive task analytics (RQ1)

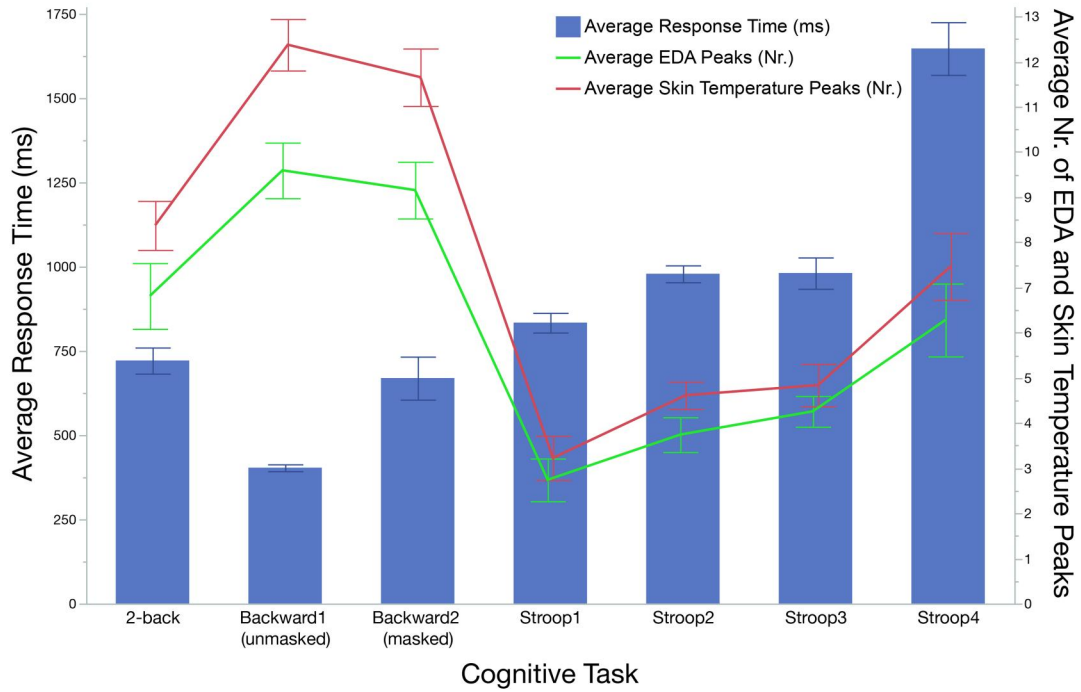
With a series of Spearman's rank-order correlations, we sought to confirm the effectiveness of our cognitive tasks in inducing cognitive workload to our participants. In turn, the induced cognitive workload serves as proof of the underlying cognitive process(es) in the respective cognitive task(s). We found a significant strong negative correlation between participants' average subjective workload (%) and their average performance score (%) across all tasks ( $r_s(238) = -.573$ ,  $p < .001$ ). This indicates that the higher the subjective workload that participants reported in a cognitive task, the worse they performed at it. Particularly, for the time-driven tasks (2-back, Backward1, and Backward2), we found (a) a significant negative correlation between participants' average response times (ms) and their average performance scores (%) ( $r_s(97) = -.372$ ,  $p < .001$ ), and (b) a significant positive correlation between average response times (ms) and average subjective workload (%) ( $r_s(97) = .379$ ,  $p < .001$ ). These correlations suggest that the slower participants responded in the time-driven tasks, the lower their average performance scores and the higher their average subjective workload.

For the participant-driven tasks, a significant negative correlation was found between participants' average response times (ms) and average performance scores (%) ( $r_s(133) = -.333$ ,  $p < .001$ ), but not between response times and subjective workload ( $r_s(133) = .123$ ,  $p = .159$ ). This suggests that the longer participants took to respond, the better they performed on average in the participant-driven tasks. These findings show that participants acted more consciously in participant-driven tasks in contrast to time-driven tasks, where the next stimulus was presented automatically. Further confirming our cognitive task manipulations, we found (a) a significant negative correlation of average EDA peaks (designating stress (Setz et al., 2009)) with average performance score ( $r_s(221) = -.218$ ,  $p < .01$ ), and (b) a significant negative one with average subjective workload ( $r_s(221) = -.318$ ,  $p < .001$ ). In line with these results, average Skin Temperature (ST) peaks (designating cognitive workload (Abdelrahman et al., 2017)) correlated significantly (a) negatively with average performance score ( $r_s(221) = -.174$ ,  $p < .01$ ), and (b) positively with subjective workload ( $r_s(221) = -.234$ ,  $p < .001$ ). These results may suggest that the higher the physiological stress levels and cognitive workload our participants experienced, the lower their average performance and the higher their subjective workload.

A one-way repeated-measures analysis of variance (ANOVA) with participants' average subjective workload (%) as dependent variable, and task type as independent variable, displayed a significant main effect for task type after a Greenhouse-Geisser correction ( $F(3.124, 103.080) = 55.446$ ,



(a) Average task performance (%) and average subjective workload (%) per task.



(b) Average response time (ms), Electrodermal Activity (EDA) and Skin Temperature (ST) peaks per task.

**Figure 5.** The 2-back, Backward1 (unmasked), Backward2 (masked), and Stroop4 were the most cognitively demanding tasks.

$p < .001$ ,  $\eta_p^2 = .627$ ). Post-hoc pairwise tests using the Bonferroni correction revealed significant differences in participants' average workload scores (%) with the Backward2 (masked) task ( $M = 58.146\%$ ,  $SD = 16.910\%$ ) rated significantly more demanding as opposed to all other tasks (Backward1:  $p < .001$  | Stroop1:  $p < .001$  | Stroop2:  $p < .001$  | Stroop3:  $p < .001$  | Stroop4:  $p < .001$ ), except for the 2-back task ( $p = .072$ , see Table 1 and Figure 5). On average,

participants systematically rated the Stroop4 task ( $M = 36.904\%$ ,  $SD = 16.874\%$ ) as the one generating the highest workload among all other Stroop tasks (Stroop1:  $p < .001$  | Stroop2:  $p < .001$  | Stroop3:  $p < .001$ ). On average, participants in Backward2, 2-back, and Stroop4 tasks reported exhibiting substantially higher subjective workload. Including Backward1 task, the same trend is observed when investigating cognitive task differences in performance scores, response



times, and physiological measures (EDA and ST peaks (Setz et al., 2009)). These findings showcase that the employed cognitive tasks induced a wide spectrum of cognitive workload as reflected in participants' varying levels of performance, subjective workload, and physiological responses (RQ1).

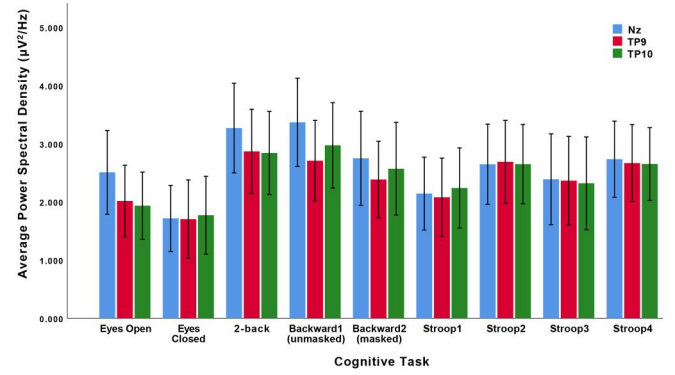
## 5.2. Cognitive process inference (RQ2)

Next, we explored whether the *BCIglass* prototype was able to infer the cognitive process(es), elicited by the cognitive task at hand, by analysing the EEG bands and relative band power. To do so, we investigated *how* the EEG relative band power differed for the Delta, Theta, Alpha and Beta bands, for all three electrodes of our *BCIglass* prototype, across all cognitive tasks, and in comparison to the baseline EEG measurements (eyes open and eyes closed). We used the average Power Spectral Density (PSD in  $\mu V^2/Hz$ ) as a measure of relative band power to perform any comparisons (see Figure 6).

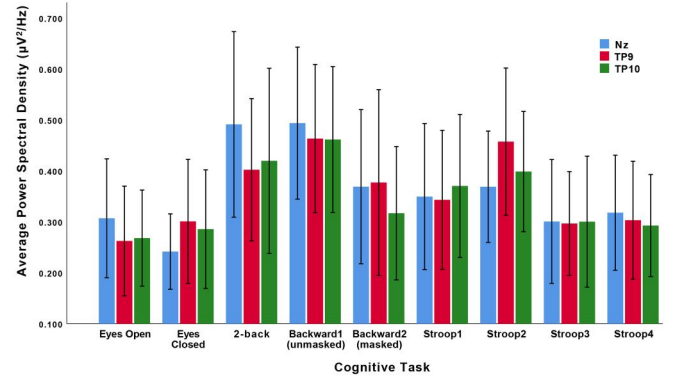
### 5.2.1. Delta band (1–4 Hz)

Three non-parametric Friedman tests displayed significant differences in the median Delta PSD captured by electrodes Nz ( $\chi_r^2(8) = 23.071, p < .01, W = .093$ ), TP9 ( $\chi_r^2(8) = 27.286, p < .01, W = .110$ ), and TP10 ( $\chi_r^2(8) = 24.241, p < .01, W = .098$ ) among the cognitive tasks and baselines. For an overview of the post-hoc pairwise comparisons between cognitive tasks, see Table 2. Post-hoc pairwise comparisons using Wilcoxon signed-rank tests for the Nz electrode showed that the median Delta PSD in the 2-back task ( $Mdn = 3.155$ ) was systematically higher than in the eyes-closed ( $Mdn = 1.514 | Z = -3.469, p < .01$ ) baseline and the Stroop1 task ( $Mdn = 1.541 | Z = -2.841, p < .01$ ). The same procedure showed that the median Delta PSD in the Backward1 task ( $Mdn = 2.866$ ) was systematically higher than in the eyes-closed baseline ( $Mdn = 1.514 | Z = -2.606, p < .01$ ), the Stroop1 task ( $Mdn = 1.541 | Z = -2.156, p < .05$ ), and the Stroop3 task ( $Mdn = 2.053 | Z = -1.999, p < .05$ ). Similarly, the median Delta PSD in the Stroop4 task ( $Mdn = 2.093$ ) was found significantly higher than in the eyes-closed baseline ( $Mdn = 1.514 | Z = -2.587, p < .05$ ). Interestingly, the median Delta PSD in the Backward2 task ( $Mdn = 1.948$ ) did not vary significantly when compared with the median Delta PSD in any other task such as the eyes-closed baseline ( $Mdn = 1.514 | Z = -1.391, p = .164$ ).

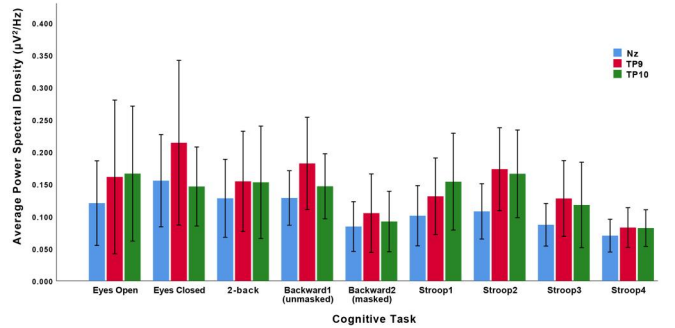
We investigated if these results were consistent for the TP9 electrode too. Post-hoc pairwise comparisons using Wilcoxon signed-rank tests for the TP9 electrode showed that the median Delta PSD in the 2-back task ( $Mdn = 2.549$ ) was significantly higher than in the eyes-open ( $Mdn = 1.711 | Z = -2.077, p < .05$ ) and eyes-closed ( $Mdn = 1.514 | Z = -3.625, p < .001$ ) baselines and the Stroop1 task ( $Mdn = 1.204 | Z = -2.528, p < .05$ ). The same procedure unveiled that the median Delta PSD in Backward1 task



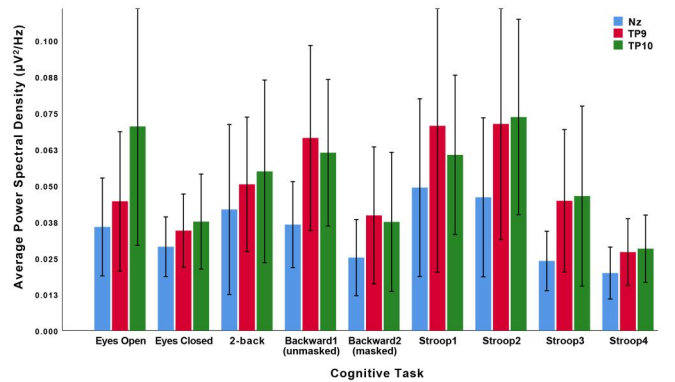
(a) Delta (1–4 Hz).



(b) Theta (4–8 Hz).



(c) Alpha (8–13 Hz).



(d) Beta (13–30 Hz).

**Figure 6.** *BCIglass* average Power Spectral Density (PSD) across all bands, electrodes, and tasks including baselines. For an overview of the significant differences among cognitive tasks, see Tables 2–4.

**Table 2.** All significant differences between cognitive tasks in median PSD ( $\mu V^2/Hz$ ) for Delta band, as captured by all three *BCIglass* electrodes.

Band	Electrode ( <i>BCIglass</i> )	High Median PSD	Low Median PSD	Wilcoxon (Z)	p-Value
Delta (1–4 Hz)	Nz	2-back (3.155)	> Eyes-closed (1.514)	–3.469	< 0.01
			> Stroop1 (1.541)	–2.841	< 0.01
		Backward1 (2.866)	> Eyes-closed (1.514)	–2.606	< 0.01
			> Stroop1 (1.541)	–2.156	< 0.05
			> Stroop3 (2.053)	–1.999	< 0.05
			> Eyes-closed (1.514)	–2.587	< 0.05
	TP9	Stroop4 (2.093)	> Eyes-open (1.711)	–2.077	< 0.05
			> Eyes-closed (1.514)	–3.625	< 0.001
		2-back (2.549)	> Stroop1 (1.204)	–2.528	< 0.05
			> Eyes-closed (1.514)	–2.528	< 0.05
		Backward1 (2.434)	> Eyes-open (1.712)	–2.116	< 0.05
			> Eyes-closed (1.514)	–.705	< 0.01
		Stroop4 (2.058)	> Stroop1 (1.204)	–2.234	< 0.05
			> Eyes-open (1.464)	–2.332	< 0.05
	TP10	2-back (2.587)	> Eyes-closed (1.389)	–3.175	< 0.01
			> Eyes-open (1.464)	–2.214	< 0.05
		Backward1 (2.666)	> Eyes-closed (1.389)	–2.567	< 0.05
			> Eyes-open (1.464)	–1.999	< 0.05
		Stroop4 (2.154)	> Eyes-closed (1.389)	–2.822	< 0.01

The 2-back, Backward1, and Stroop4 cognitive tasks generated substantially higher median Delta PSD, as opposed to eyes-open/closed baselines and less-demanding internal-processing tasks (e.g., Stroop1).

**Table 3.** All significant differences between cognitive tasks in median PSD ( $\mu V^2/Hz$ ) for Theta band as captured by the Nz and TP9 *BCIglass* electrodes.

Band	Electrode ( <i>BCIglass</i> )	High Median PSD	Low Median PSD	Wilcoxon (Z)	p-Value
Theta (4–8 Hz)	Nz	2-back (.284)	> Eyes-open (.194)	–2.018	< 0.05
			> Eyes-closed (.226)	–2.077	< 0.05
		Backward1 (.399)	> Eyes-open (.194)	–3.116	< 0.01
			> Eyes-closed (.226)	–3.175	< 0.01
			> Stroop3 (.223)	–2.234	< 0.01
			> Stroop4 (.240)	–2.802	< 0.01
	TP9	Backward1 (.330)	> Eyes-open (.129)	–2.998	< 0.01
			> Eyes-closed (.181)	–2.587	< 0.05
			> Stroop4 (.247)	–2.548	< 0.01
			> Eyes-open (.129)	–2.587	< 0.05
		Stroop2 (.348)	> Eyes-closed (.181)	–2.352	< 0.05

The 2-back and Backward1 cognitive tasks generated substantially higher median Theta PSD, as opposed to eyes-open/closed baselines, and less-demanding decision-making, willed-attention and working-memory tasks (e.g., Stroop3).

**Table 4.** All significant differences between cognitive tasks in median PSD ( $\mu V^2/Hz$ ) for Alpha band as captured by the TP9 *BCIglass* electrode.

Band	Electrode ( <i>BCIglass</i> )	High Median PSD	Low Median PSD	Wilcoxon (Z)	p-Value
Alpha (8–13 Hz)	TP9	Backward1 (.110)	> Backward2 (.051)	–3.018	< 0.01
		Stroop2 (.093)		–2.606	< 0.01
		Backward1 (.110)	> Stroop4 (.063)	–3.153	< 0.01
		Stroop2 (.093)		–2.410	< 0.05

The Backward2 and Stroop4 cognitive tasks generated substantially lower median Alpha PSD, as opposed to less cognitively demanding tasks (e.g., Stroop2).

( $Mdn = 2.434$ ) was significantly higher than in the eyes-closed baseline ( $Mdn = 1.514$ ,  $Z = -2.528$ ,  $p < .05$ ), but no significant difference was observed between the median Delta PSD in Backward2 task ( $Mdn = 1.886$ ) and in any other task or baseline such as the eyes-closed baseline ( $Mdn = 1.514$ ,  $Z = -1.176$ ,  $p = .240$ ). However, the same procedure revealed that the median Delta PSD in the Stroop4 task ( $Mdn = 2.058$ ) was systematically higher than in the eyes-open ( $Mdn = 1.712$ ,  $Z = -2.116$ ,  $p < .05$ ) and eyes-closed ( $Mdn = 1.514$ ,  $Z = -.705$ ,  $p < .01$ ) baselines and in the Stroop1 task ( $Mdn = 1.204$ ,  $Z = -2.234$ ,  $p < .05$ ).

Finally, we looked into the measurements of the TP10 electrode. A series of post-hoc pairwise comparisons using Wilcoxon signed-rank tests for the TP10 electrode showed

that the median Delta PSD in the 2-back task ( $Mdn = 2.587$ ) was significantly higher than in the eyes open ( $Mdn = 1.464$ ,  $Z = -2.332$ ,  $p < .05$ ) and eyes closed ( $Mdn = 1.389$ ,  $Z = -3.175$ ,  $p < .01$ ) baselines. Similarly, the median Delta PSD in the Backward1 task ( $Mdn = 2.666$ ) was found substantially higher than in the eyes-open ( $Mdn = 1.464$ ,  $Z = -2.214$ ,  $p < .05$ ) and eyes-closed ( $Mdn = 1.389$ ,  $Z = -2.567$ ,  $p < .05$ ) baselines. Interestingly, the same procedure did not reveal any significant differences between the median Delta PSD in the Backward2 task ( $Mdn = 1.752$ ) and in any other task or baseline such as the eyes closed ( $Mdn = 1.389$ ,  $Z = -1.195$ ,  $p = .232$ ). However, the tests showed that the median Delta PSD in the Stroop4 task ( $Mdn = 2.154$ ) was systematically higher than in the

eyes-open ( $Mdn = 1.464 | Z = -1.999, p < .05$ ) and eyes-closed ( $Mdn = 1.389 | Z = -2.822, p < .01$ ) baselines. These results demonstrate that the Delta band power, as measured by the *BCIglass* prototype, displayed significant fluctuations almost among all cognitive tasks, indicating varying levels of increased attention to internal processing (Harmony et al., 1996) (RQ2).

### 5.2.2. Theta band (4–7 Hz)

Three non-parametric Friedman tests displayed significant differences in the median Theta PSD ( $\mu V^2/Hz$ ) captured by electrodes Nz ( $\chi_r^2(8) = 17.127, p < .05, W = .069$ ) and TP9 ( $\chi_r^2(8) = 20.912, p < .01, W = .084$ ), but not in the median Theta PSD captured by TP10 ( $\chi_r^2(8) = 15.045, p = .058, W = .061$ ). For an overview of the post-hoc pairwise comparisons between cognitive tasks, see Table 3. Post-hoc pairwise comparisons using Wilcoxon signed-rank tests for the Nz electrode showed that the median Theta PSD in the 2-back task ( $Mdn = .284$ ) was systematically higher than in the eyes-open ( $Mdn = .194 | Z = -2.018, p < .05$ ) and eyes-closed ( $Mdn = .226 | Z = -2.077, p < .05$ ) baselines. The same procedure unveiled that the median Theta PSD in Backward1 task ( $Mdn = .399$ ) was substantially higher than in the eyes-open ( $Mdn = .194 | Z = -3.116, p < .01$ ) and eyes-closed ( $Mdn = .226 | Z = -3.175, p < .01$ ) baselines, but also higher than in the Stroop3 task ( $Mdn = .223 | Z = -2.234, p < .01$ ) and surprisingly the Stroop4 task ( $Mdn = .240 | Z = -2.802, p < .01$ ). Interestingly, the same tests displayed no difference in the median Theta for Backward2 task ( $Mdn = .228$ ) when compared with any other task or baseline, such as eyes closed ( $Mdn = .226, | Z = -1.568, p = .117$ ). We also investigated if these results were consistent for the TP9 electrode too. A series of post-hoc pairwise comparisons using Wilcoxon signed-rank tests for the TP9 electrode displayed no significant differences in the median Theta PSD for the 2-back task ( $Mdn = .278$ ) when compared with the median Theta PSD in any other task or baseline, such as eyes closed ( $Mdn = .181 | Z = -1.627, p = .104$ ). In contrast, the same tests displayed a significantly higher median Theta PSD for Backward1 task ( $Mdn = .330$ ), as opposed to the eyes-open ( $Mdn = .129 | Z = -2.998, p < .01$ ) and eyes-closed ( $Mdn = .181 | Z = -2.587, p < .05$ ) baselines, but also higher than the median Theta PSD for Stroop4 task ( $Mdn = .247 | Z = -2.548, p < .01$ ). However, the same procedure did not display any significant difference between the median Theta PSD for the Backward2 task ( $Mdn = .185$ ) and the median Theta PSD for any other task or baseline, such as eyes closed ( $Mdn = | Z = -.764, p = .445$ ). Interestingly, the same tests revealed that the median Theta PSD for the Stroop2 task ( $Mdn = .348$ ) was systematically higher than in the eyes-open ( $Mdn = .129 | Z = -2.587, p < .05$ ) and eyes-closed baselines ( $Mdn = .181 | Z = -2.352, p < .05$ ). These results showcase that cognitive tasks involving decision-making in oddball paradigms with willed attention (i.e., Backward1) (Rajan et al., 2019) and working memory (i.e., 2-back) (Klimesch, 1999; Mecklinger et al., 1992) evoked stronger Theta band-power fluctuations than other tasks, as measured by the *BCIglass*

prototype. However, we did not observe a linear increase in Theta PSD with increasing stimulus interference (i.e., Stroop tasks) (Hanslmayr et al., 2008) (RQ2).

### 5.2.3. Alpha band (8–12 Hz)

Three non-parametric Friedman tests revealed significant differences in the median Alpha PSD ( $\mu V^2/Hz$ ) captured by electrode TP9 ( $\chi_r^2(8) = 15.656, p < .05, W = .063$ ) among the cognitive tasks and baselines, but no significant differences in the median Alpha PSD captured by the Nz ( $\chi_r^2(8) = 13.376, p = .100, W = .054$ ) and the TP10 ( $\chi_r^2(8) = 10.323, p = .243, W = .042$ ) electrodes. For an overview of the post-hoc pairwise comparisons between cognitive tasks, see Table 4. Post-hoc pairwise comparisons using Wilcoxon signed-rank tests for the TP9 electrode unveiled that the median Alpha PSD in the Backward2 task ( $Mdn = .051$ ) was significantly lower than in the Backward1 ( $Mdn = .110 | Z = -3.018, p < .01$ ) and the Stroop2 ( $Mdn = .093 | Z = -2.606, p < .01$ ) tasks. The same procedure revealed a substantially lower median Alpha PSD in the Stroop4 task ( $Mdn = .063$ ) when compared with the Backward1 ( $Mdn = .110 | Z = -3.153, p < .01$ ) and the Stroop2 ( $Mdn = .093 | Z = -2.410, p < .05$ ) tasks. Interestingly, the median Alpha PSD in the 2-back task did not differ significantly from the median Alpha PSD ( $Mdn = .1072$ ) in any of the other tasks or baselines captured by the TP9 electrode such as in the eyes-closed ( $Mdn = .103 | Z = -.412, p = .681$ ) baseline. These findings display a systematically lower Alpha PSD in tasks designed to induce high cognitive workload (i.e., Backward2, Stroop4) (Klimesch et al., 1993). Interestingly, this trend was only observed in the Alpha band power captured by the TP9 electrode of the *BCIglass* prototype (RQ2).

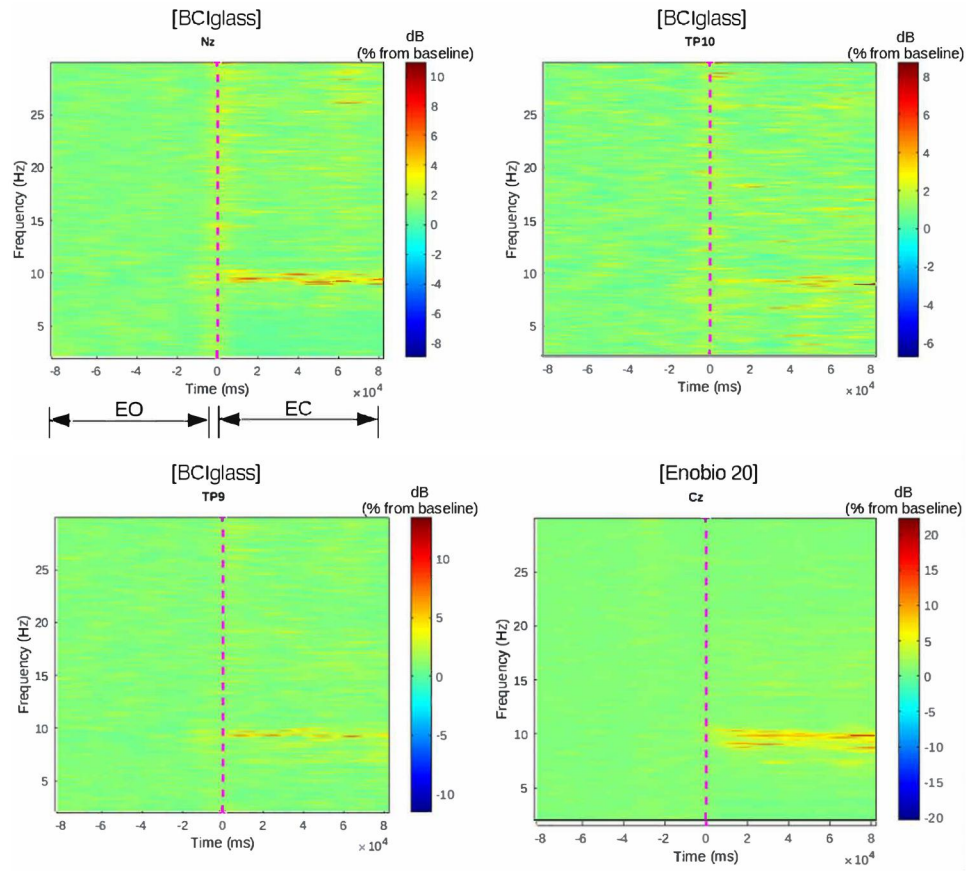
### 5.2.4. Beta band (12–30 Hz)

Three non-parametric Friedman tests revealed no significant differences in the median Beta PSD captured by electrodes Nz ( $\chi_r^2(8) = 12.604, p = .126, W = .053$ ), TP9 ( $\chi_r^2(8) = 11.804, p = .160, W = .049$ ), and TP10 ( $\chi_r^2(8) = 13.076, p = .109, W = .054$ ) among all cognitive tasks and baselines. These results were somewhat expected since the Beta band is evoked mostly in motor execution/preparation tasks (Crone et al., 1998; Vourvopoulos et al., 2019) (RQ2).

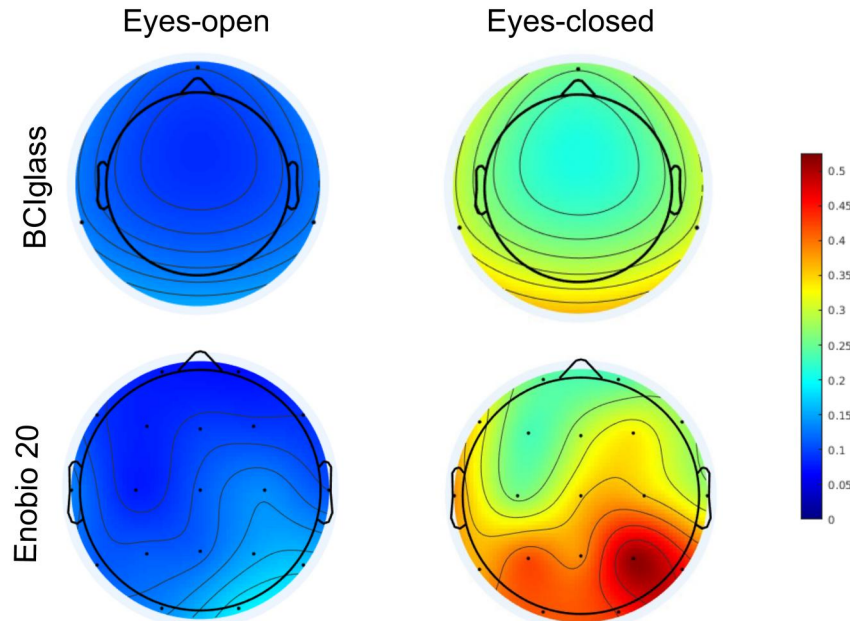
## 5.3. EEG topology comparison (RQ3)

Initially, we compared the resting-state Alpha power between the two systems/topologies when the participants performed a simple “eyes-open/eyes-closed” task. It is well known that Alpha EEG activity is dominant in healthy individuals during an eyes-closed resting condition, and is suppressed with visual stimulation (Adrian & Matthews, 1934; Jasper, 1936). As anticipated, we detected an increase in relative Alpha band power during eyes-closed with the Enobio 20 system, but also with all the *BCIglass* electrodes (see Figure 7). This is a key finding since it enables us to validate the *BCIglass* system with standard methodological





(a) Time/Frequency plots during eyes-open (EO) and eyes-closed (EC) resting state for *BCIglass* (Nz, TP9 & TP10) and Enobio 20 (Cz).



(b) Alpha power spatial distribution.

**Figure 7.** An increase in the relative Alpha band power is observed between the eyes-open and eyes-closed resting-state conditions for both systems. This enables us to validate the *BCIglass* prototype against standard methodological approaches in a dominant EEG feature such as relative resting-state Alpha.

approaches in a dominant EEG feature such as relative resting-state Alpha. In fact, resting-state Alpha is used in investigating major psychiatric disorders (e.g., Attention-Deficit/Hyperactivity Disorder—ADHD, addiction, schizophrenia,

depression, anxiety, Obsessive Compulsive Disorder—OCD, autism, Post-Traumatic Stress Disorder—PTSD, see (Newson & Thiagarajan, 2018) for an overview), as well as in mindfulness and meditation studies (Başar et al., 2001;

Klimesch, 1999), hence increasing the potential use cases of a ubiquitous *BCIglass* system.

For brevity, we utilised the composite measure of the Engagement Index (EI) known for correlating with participants' self-reported task engagement (Kamzanova et al., 2014; Pope et al., 1995). The Cz and Pz electrodes are located over the central and parietal lobes based in the 10-10 system (see Figure 2(a)). We opted for a middle scalp location as a compromise between the predominantly posterior distribution of Alpha band power and the frontal lobe involvement in working memory (Rypma & D'Esposito, 1999). First, a series of non-parametric Spearman's rank-order correlations were conducted between the three electrodes of our prototype (Nz, TP9, TP10) and the two selected electrodes of Enobio 20 (Cz, Pz) to determine if there is a relationship in the average EI measured by the two systems/topologies. Across all cognitive tasks and baselines, we found significant and positive correlations in average measured EI between the Nz and Cz electrodes ( $r_s(242) = .177, p < .01$ ), between the TP9 and Cz electrodes ( $r_s(242) = .215, p < .01$ ) and between the TP10 and Cz electrodes ( $r_s(242) = .214, p < .01$ ), as well as between the TP9 and Pz electrodes ( $r_s(242) = .128, p < .05$ ). From the outset, these results may imply that both systems/topologies might be aligned when it comes to measuring a composite EEG product such as EI across all cognitive tasks, including the baselines (see Figure 8).

Next, we investigated for both systems the relationship between EI and subjective measures of effort and workload, such as the constructs that comprise the NASA TLX index. For this, we performed a series of non-parametric Spearman's rank-order correlations with EI measured by the three electrodes of our prototype (Nz, TP9, TP10) and by

the two selected electrodes of Enobio 20 (Cz, Pz). Interestingly, for our prototype we discovered three significant and negative correlations between average EI measured by: (1) the Nz electrode and average subjective physical demand ( $r_s(242) = -.177, p < .01$ ), (2) the TP10 electrode and average subjective physical demand ( $r_s(242) = -.141, p < .05$ ), and (3) the TP10 electrode and average subjective effort ( $r_s(242) = -.139, p < .05$ ). Conversely, we discovered one significant and positive correlation between average EI measured by the Cz (Enobio 20) electrode and average subjective physical demand ( $r_s(242) = .158, p < .05$ ). These findings showcase that average EI measured by both systems correlates with subjective measures of effort and physical demand (Kamzanova et al., 2014; Pope et al., 1995) (RQ3).

As a measure of “agreement” between the two systems/topologies, we compared *how similar* are the EI distributions of measurements, produced by the electrodes of our *BCIglass* topology, with the EI distributions produced by the (selected) electrodes of Enobio 20. To do so, we performed a series of pairwise related-samples Friedman's two-way analyses of variance by ranks for each electrode pair, comprised of one electrode for our prototype (Nz, TP9, TP10) and one of the selected ones for Enobio 20 (Cz, Pz). The null hypothesis (H0) of the specified statistical test assumes that the distributions between two samples of the same population—EI measurements by *BCIglass* and Enobio 20 for the same participants—are the same (Pereira et al., 2015; Siegel, 1956). The analyses unveiled that the *BCIglass* Nz electrode measured EI in a different fashion than the Enobio 20 Cz ( $\chi^2_r(1) = 11.174, p < .01$ ) and Pz ( $\chi^2_r(1) = 16.926, p < .001$ ) electrodes did, respectively. Interestingly, comparisons between the EI distributions of TP9 with Cz ( $\chi^2_r(1) =$

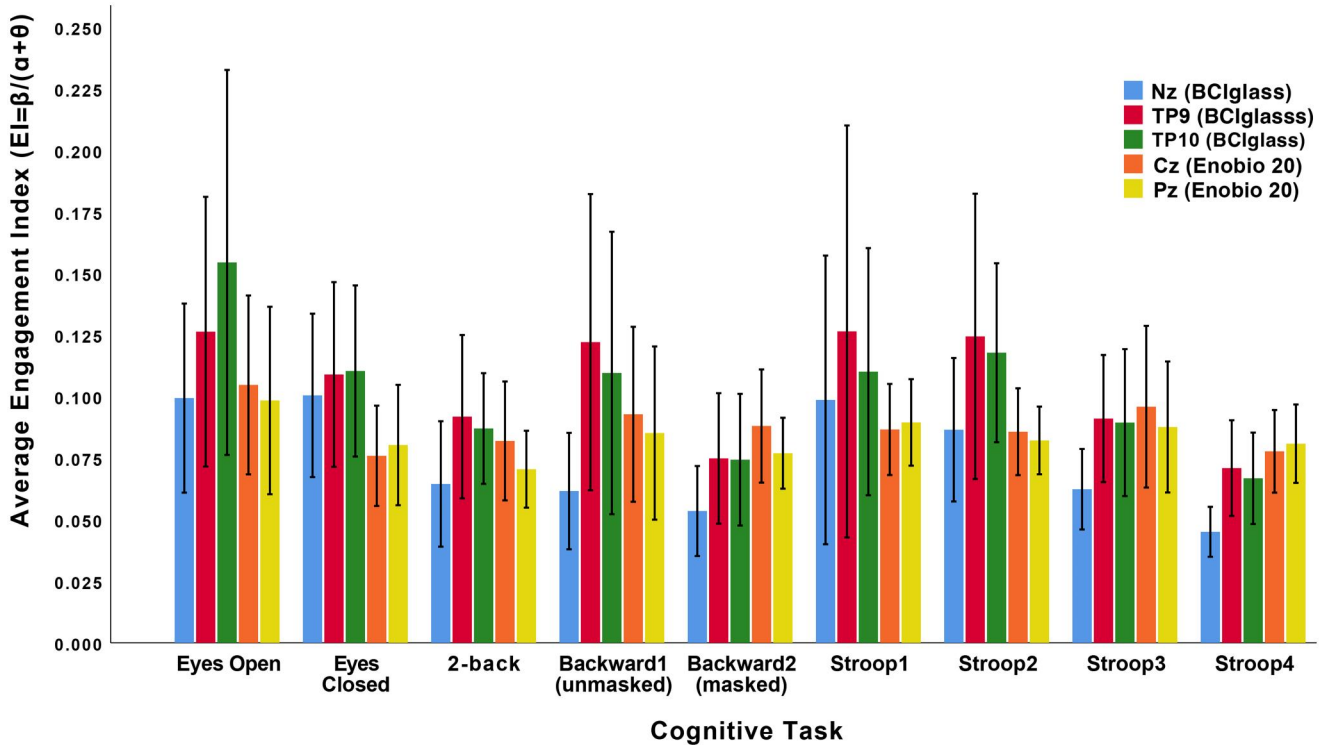


Figure 8. Engagement Index for each task as recorded by the *BCIglass* (Nz, TP9 & TP10) and Enobio 20 (Cz, Pz) electrodes.

.810,  $p = .368$ ) and with Pz ( $\chi^2_r(1) = .000, p = 1.0$ ) as well as, comparisons between the EI distributions of TP10 with Cz ( $\chi^2_r(1) = 2.793, p = .95$ ) and with Pz ( $\chi^2_r(1) = .264, p = .607$ ), respectively, retained the H0. Thus, except for the Nz electrode, the TP9 and TP10 electrodes of our *BCIglass* electrode topology, measure EI in the same way as the Cz and Pz electrodes of an EEG-cap electrode topology. These findings demonstrate that our experimental *BCIglass* electrode topology can capture EEG activity induced by a wide variety of cognitive tasks similarly to a higher-resolution EEG-cap topology (RQ3).

Finally, we trained a series of classifier models to predict the cognitive task at hand, using the PSD as features, for both electrode topologies, including data captured from all electrodes for both systems (i.e., three plus two for reference and ground for *BCIglass*, and 20 for Enobio 20). Note that our aim here is *not* to create a general model but rather compare between the two systems and electrode topologies (RQ3). As described in Section 4.5, the EEG data had first been pre-processed by applying the respective filters, re-referencing, and ICA techniques to extracting the PSD for all bands across all cognitive tasks. To classify the cognitive task at hand, we trained (a) Support Vector Machine (SVM), (b) K-nearest neighbour (KNN), (c) 4-layer Convolutional Neural Network (CNN), and (d) Extreme Gradient Boosting (XGBoost) models, based on prominent classification algorithms for BCIs (Lotte et al., 2018). We performed an 80–20 data split between training and validation, and computed average accuracy scores from 20 different random trials in each case. We trained the aforementioned models both within participants (one model/participant) and across participants (one model for all). The reason why we did not perform K-fold cross-validation is that sometimes the dataset is too small to cast into higher K-fold, and smaller K values usually lead to insufficient training data and influence the accuracy scores. Instead, we performed a grid search on the accuracy values that yielded a  $K = 1$  value.

- **SVM.** We used the *svm* classifier from *scikit-learn*.<sup>16</sup> We initialized it with Radial Basis Function kernel (RBF) by setting *kernel*="rbf" and mapped inputs into higher dimensions to fit a non-linear boundary for decisions. The regularization parameter, C, was set to 1.0 to balance the trade-off between a low training error and a low testing error. The gamma parameter, which influences the extent of influence of a single training example, was set to "scale," meaning it uses  $1/(n_{features} * X.var())$  as its value.
- **KNN.** We used the *KNeighborsClassifier* from *scikit-learn* to create a k-Nearest Neighbors (k-NN) classifier.<sup>17</sup> Based on our preliminary benchmark, we found that the score was the best when initialized with one neighbor by setting  $n_{neighbors} = 1$ . This means the classification decision is based on the single closest training example. We set the weights parameter to "distance," which adjusts the influence of each neighbor based on their distance, giving closer neighbors more influence on the classification decision. We then left all other parameters as default.

- **CNN.** We assembled a sequential model architecture using Keras.<sup>18</sup> The network starts with a *Conv1D* layer, equipped with 344 filters, a kernel size of 1, and is initialized with the "he\_uniform" initializer. It is regulated by L2 normalization to reduce overfitting. Batch normalization is then applied to maintain stability in the activations. A pooling method is then used to reduce the dimensionality of the parameters and control overfitting further. Two dense layers are then applied, each activated by a rectified linear unit (ReLU) with a follow-up dropout function in rate of 0.25. The dropout helps remove weak connections and further prevents overfitting. The final output layer has 7 units in the first trial and 3 units in the second with a *softmax* activation function for classification. The network was compiled with the Adam optimizer, utilizing a learning rate of 0.01, and *categorical\_crossentropy* was chosen as the loss function. We trained the network with 15 epochs and a batch size of 256. Since we have a relatively small dataset, a shallow network (i.e., 4-layer CNN) could further reduce the risk of overfitting. For a detailed architecture of the CNN model, see Table 5.
- **XGBoost.** We used the off-the-shelf version of the *XGBoost* classifier.<sup>19</sup> The workflow of *XGBoost* (Extreme Gradient Boosting) begins with initializing a series of decision trees. Each new tree is built to correct the errors made by the previous trees and enhance the model's overall accuracy. The network utilizes a tree learning algorithm to handle sparse data and a weighted quantile sketch for efficient approximate tree learning. In the *XGBoost* classifier configuration, we set *max\_depth* as 6, and *learning\_rate* (or eta) to 0.3. We used *gbtree* as our booster, with *subsample* and *colsample\_bytree* both at 1.0. The *gamma* parameter was 0, *min\_child\_weight* was 1, and both *reg\_alpha* and *reg\_lambda* were 0.

Initially, we attempted to train classifiers that classify all seven distinct cognitive tasks but both systems (*BCIglass* & Enobio 20) performed poorly (see Table 6). The best average classification accuracy achieved for all seven cognitive tasks was 22.31% for the *BCIglass* topology and 30.89% for the Enobio 20, when training/testing an SVM with RBF kernel and a 4-layer CNN, respectively (see Tables 6). Due to scarce data, we instead resorted to predicting the type of the cognitive task at hand: (1) 2-back class (2) Backward

**Table 5.** The architecture of the 4-layer Convolutional Neural Network (CNN) trained to classify the type (class) of the cognitive task at hand on Power Spectral Density (PSD).

Nr. Layer (type)	Output Shape	Param. #
1 <i>conv1d</i> (Conv1D)	(None, 1, 344)	688
<i>batch_normalization</i> (BatchNo)	(None, 1, 344)	1376
<i>max_pooling1d</i> (MaxPooling1D)	(None, 1, 172)	0
2 <i>dense</i> (Dense)	(None, 1, 4,096)	707,584
<i>dropout</i> (Dropout)	(None, 1, 4096)	0
3 <i>dense_1</i> (Dense)	(None, 1, 2,048)	8,390,656
<i>dropout_1</i> (Dropout)	(None, 1, 2048)	0
4 <i>dense_2</i> (Dense)	(None, 1, 3)	6147
		Total params: 9,106,451
		Trainable params: 9,105,763
		Non-trainable params: 688



**Table 6.** First attempt (7 classes): Average validation & testing Accuracy (a), Precision (P) and Recall (R) in classifying the *cognitive task* at hand (7 cognitive tasks/classes) for both topologies with different models—data captured from all electrodes included for both systems.

7 Classes Classifier	Within Participants						Across Participants					
	Enobio 20			BCIglass			Enobio 20			BCIglass		
	A (%)	P (%)	R (%)	A (%)	P (%)	R (%)	A (%)	P (%)	R (%)	A (%)	P (%)	R (%)
SVM (RBF)	17.62	14.29	11.11	8.47	8.86	6.05	21.22	18.29	14.49	<b>22.31</b>	<b>13.30</b>	<b>10.41</b>
KNN ( $K=1$ )	15.86	13.48	8.89	10.67	10.39	7.26	22.67	17.67	12.59	14.70	14.29	8.81
CNN (4 layers)	6.82	7.14	5.11	5.38	4.94	4.63	<b>30.89</b>	<b>26.19</b>	<b>7.58</b>	20.00	13.21	4.64
XGBoost	12.67	14.29	8.17	12.50	12.05	6.90	27.76	28.57	6.37	16.42	13.89	3.91

SVM with RBF kernel displayed the highest accuracy (22.31%) for BCIglass with Power Spectral Density (PSD) as features, 8.58% lower than Enobio 20 using a 4-layer CNN. Both systems performed poorly due to scarce data to reliably classify 7 distinct cognitive task classes. Significant differences are highlighted in bold font for a  $p$ -value  $<.05$ .

**Table 7.** Second attempt (3 classes): Average validation & testing Accuracy (a), Precision (P) and Recall (R) in classifying the *cognitive task type* at hand (grouping 7 cognitive tasks to 3 types/classes: Backward Masking, 2-back and Stroop tasks) for both topologies with different models—data captured from all electrodes included for both systems.

3 Classes Classifier	Within Participants						Across Participants					
	Enobio 20			BCIglass			Enobio 20			BCIglass		
	A (%)	P (%)	R (%)	A (%)	P (%)	R (%)	A (%)	P (%)	R (%)	A (%)	P (%)	R (%)
SVM (RBF)	64.71	69.57	42.11	64.85	62.50	42.86	42.31	37.50	30.77	40.21	38.71	37.50
KNN ( $K=1$ )	88.02	78.57	84.62	59.58	51.61	47.06	79.85	75.86	68.75	59.20	57.14	43.24
CNN (4 layers)	56.92	54.55	43.90	62.07	58.06	48.65	50.00	45.16	36.84	<b>79.79</b>	<b>77.78</b>	<b>65.63</b>
XGBoost	84.23	82.14	74.19	53.79	53.57	37.50	<b>88.00</b>	<b>82.31</b>	<b>75.00</b>	67.00	62.07	52.94

A 4-layer CNN displayed the highest accuracy for BCIglass with Power Spectral Density (PSD) as features, 8.21% lower than Enobio 20 using XGBoost. Significant differences are highlighted in bold font for a  $p$ -value  $<.05$ .

Masking class, and (3) Stroop class (see Table 7). For both systems, the highest accuracy in predicting the cognitive task class was achieved when training classifiers across participants. The best average classification accuracy achieved was 79.79% for the BCIglass topology and 88% for the Enobio 20, when training/testing a 4-layer CNN and an XGBoost model, respectively. With a low spatial electrode resolution, at the periphery of the skull, our BCIglass topology achieved a cognitive task type classification accuracy of  $\sim 8\%$  lower than that of a higher-resolution EEG-cap topology (RQ3). In other words, the BCIglass topology yields an improved task-type classification accuracy-over-electrode ratio ( $79.79\% / (3 + 1_{\text{gnd}} + 1_{\text{ref}}) = 15.958 \text{ \%/electrode}$ ) when compared to Enobio 20 ( $88\% / 20 = 4.4 \text{ \%/electrode}$ ).

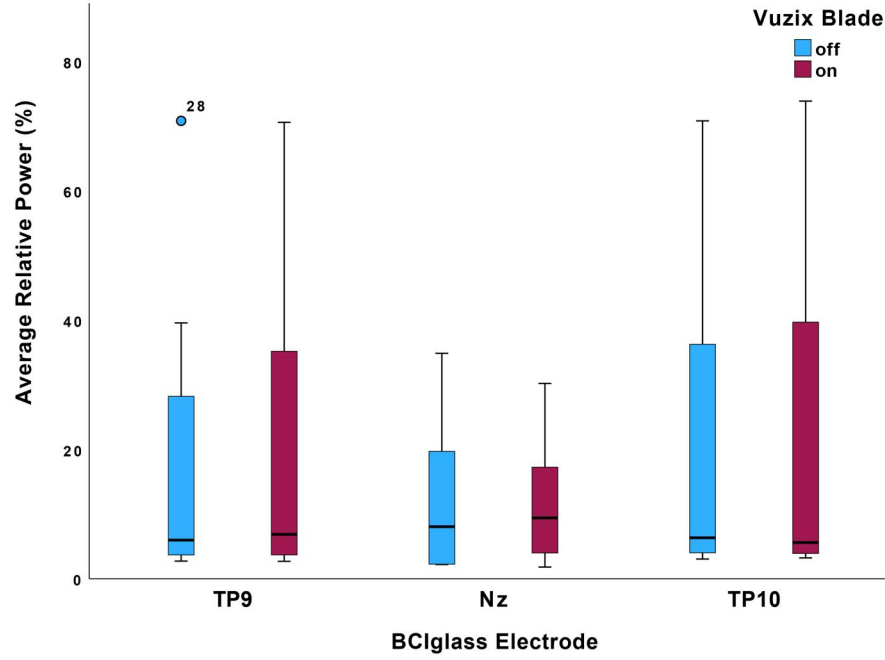
#### 5.4. Pilot study in the wild

We conducted a limited pilot study with one participant ( $N=1$ , female, 32 years old) in the wild to investigate whether the BCIglass is capable of capturing EEG activity that indicates cognitive processes outside the lab. The participant was recruited from the premises of our University with no history of neurological disorders. In a brief session, we instructed the participant on how to use the BCIglass (e.g., apply conductive paste) and the required software (e.g., “OpenBCI\_GUI”) to collect their EEG activity data. The participant tested the BCIglass in their free time when at home, and in activities that require composite levels of attention, visual processing, memory recall, decision-making, emotional processing, and motor control: (1) correcting exams (1 hour) (Davis et al., 2011), (2) PC gaming (1 hour) (Kühn et al., 2011; Moisa et al., 2017), and (3) watching a movie (1 hour) (Nie et al., 2011). The “correcting exams” activity

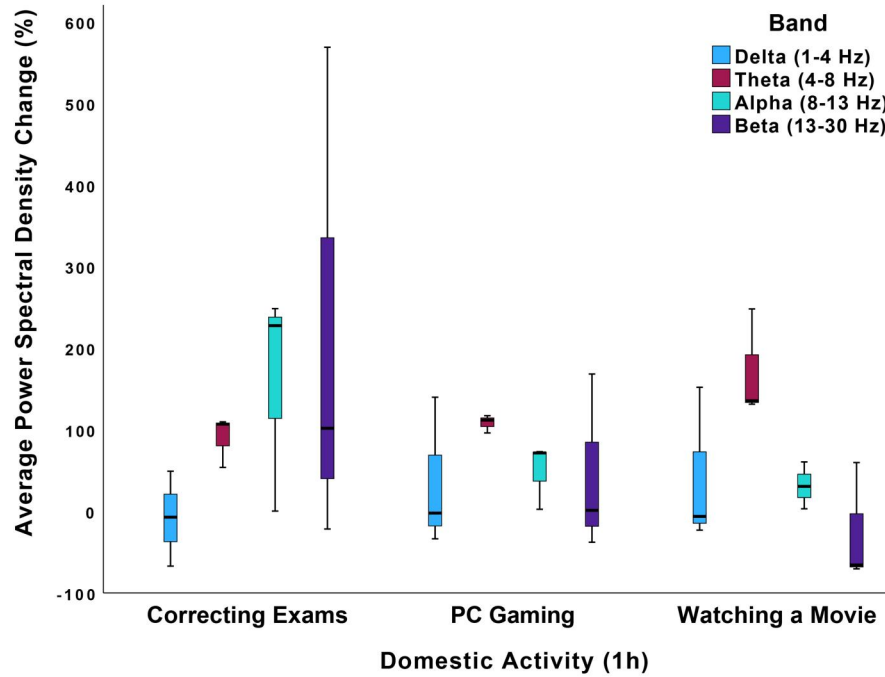
involved manually grading physical exam copies for 1 hour, while checking a computer screen displaying the solutions. The “PC gaming” activity involved playing the “EVE Online”<sup>20</sup> space simulation game for 1 hour, and while performing low intensity tasks (e.g., asteroid mining). The “watching movie” activity involved watching 1 hour of the “Saving Private Ryan (1998)”<sup>21</sup> war movie, known for its graphic and realistic portrayal of war. Upon delivering the BCIglass to the participant, we captured 2-min resting state baselines (eyes open) with Vuzix Blade on/off. We captured the 2-min resting state baselines twice in a counterbalanced order (i.e., on–off–off–on) to cancel out any carry-over effects.

First, we empirically assessed whether an active Vuzix Blade HMD has an influence on the EEG signal recorded by the BCIglass prototype during the 2-min resting states. A pairwise related-samples Friedman’s two-way analysis of variance by ranks displayed no significant difference in the average relative power for all electrode-band pairs between Vuzix Blade on ( $\bar{R}_{\text{on}} = 1.58$ ) and off ( $\bar{R}_{\text{off}} = 1.42$ ) states ( $\chi^2_r(1) = .667, p = .414$ ). Thus, by maintaining the  $H_0$ , we showcase that the BCIglass captures EEG activity in the same fashion and irrespective of whether Vuzix Blade is powered on or off (see Figure 8). This finding confirms our earlier hypothesis in that any EMF produced by the Vuzix Blade HMD will lie far above the usable EEG spectrum (1–100 Hz) to affect it.

Next, we extracted the power spectral density (PSD) for each of the EEG bands (Delta, Theta, Alpha and Beta) during the three activities (correcting exams, PC gaming and watching a movie), and we computed the percent (%) change for each band (Equation 1) when compared to an initial (eyes-open) resting-state session which served as a baseline. Here, we performed only minimal pre-processing



(a) Average relative power (%) per *BCIglass* electrode during eyes-open resting state when the Vuzix Blade is switched ON and OFF. The measurements are highly similar across all *BCIglass* electrodes.



(b) EEG band power change (%) in median electrode power across three activities at home. In “Correcting Exams,” Alpha (Mdn = 227 %) and Beta (Mdn = 102 %) band power are mostly higher compared to “PC Gaming” and “Watching a Movie.”

**Figure 9.** We empirically confirm that the Vuzix Blade operation does not influence the *BCIglass* measurements. The previously detected EMF (max. 382 mW/m<sup>2</sup> at 2.4–2.5 GHz) lies way above the usable EEG spectrum (1–100 Hz) to have any effect.

to extract the PSD within the limits of the EEG bands, thus band-passing between 1 and 40 Hz. We opted for this to maintain ecological validity and simulate the real-time analysis that can be performed in real-world applications (e.g., excluding ICA).

$$\text{Percent Change}_{\text{PSD}} = \left( \frac{\text{PSD}_{\text{task}} - \text{PSD}_{\text{baseline}}}{\text{PSD}_{\text{baseline}}} \right) \times 100 \quad (1)$$

In terms of EEG band power change (%), we observe differences across the three activities in median electrode

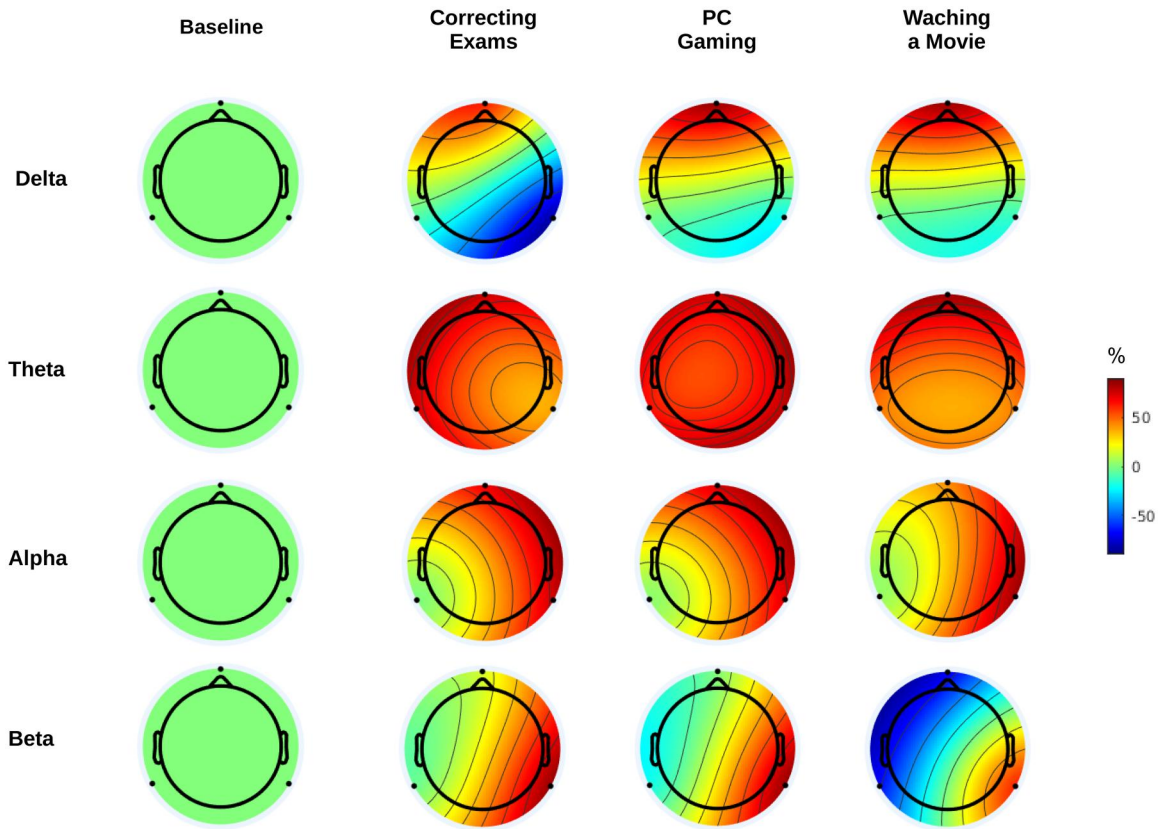


**Figure 10.** Power Spectral Density (PSD) change (%) distribution from resting-state baseline (eyes-open) for Delta (1–4 Hz), Theta (4–8 Hz), Alpha (8–13 Hz) and Beta (13–30 Hz) bands across three 1-h tasks performed in the wild: (a) correcting exams, (b) PC gaming, and (c) watching a movie.

power (see Figure 9(b)) but also in spatial distribution (see Figure 10). Specifically, during “correcting exams,” we observe that, for all *BCIglass* electrodes, relative Alpha (Mdn = 227%) and Beta (Mdn = 102%) band power are mostly higher compared to “PC gaming” and “watching a movie” (see Figure 9(b)). The Alpha band is typically suppressed during visual stimulation, such as when gaming or watching a movie (Adrian & Matthews, 1934; Jasper, 1936). The increased relative Beta band power observed in “correcting exams” can be attributed to motor preparation and execution such as hand movement (e.g., browsing through exam pages, checking solutions) (Crone et al., 1998). Interestingly, we observe an increase in relative Theta band power in the “watching a movie” condition that could be ascribed to increased emotional processing (Messerotti Benvenuti et al., 2017). The relationship between Alpha, Beta and Theta bands has been studied in the context of various cognitive and psychological states (Hanslmayr et al., 2008; Klimesch et al., 1993; Mecklinger et al., 1992; Rajan et al., 2019). In general, modulation of the Alpha, Beta and Theta ratio is often associated with cognitive functioning and may indicate a state of relaxation and focused attention (Harmony et al., 1996), plus it is often used in neurofeedback (Jurewicz et al., 2018; Zoefel et al., 2011). Thus, our *BCIglass* prototype appears to be capable of capturing EEG activity related to everyday-life activities performed in the wild. However, further research is required to reliably prove the capabilities of *BCIglass* in the wild.

## 6. Discussion

Our findings suggest that a sparse EEG-electrode topology, constrained at the periphery of the skull, can detect cognitive workload, can infer cognitive processes and can measure EEG activity almost in a similar manner to a higher-resolution topology of a research-grade system (Enobio 20). Early results from a limited pilot study in the wild indicate that all these may be possible in the complex settings of everyday life. Moreover, the *BCIglass* prototype achieved an improved accuracy-over-electrode ratio in predicting the class of the cognitive-task at hand in comparison to Enobio 20. These are encouraging findings in the quest of designing cognition-aware systems for everyday use.

### 6.1. Internal validity of cognitive tasks and hints to ecological validity

Although our cognitive tasks were based on paradigms extensively used in cognitive psychology and neuroscience, we had no empirical evidence about their effectiveness in inducing cognitive workload and invoking cognitive processes (RQ1). To establish this, we utilized objective, subjective, and physiological measures of (cognitive) performance, workload, and stress. From the outset, we confirmed known phenomena in literature, such as strong relationships among high subjective workload (Young et al., 2015), physiological stress (Setz et al., 2009), and physiological cognitive



workload (Abdelrahman et al., 2017), all linked to lower cognitive performance (Hart & Staveland, 1988). Overall, the employed measures converge in that the top four most cognitively demanding tasks (out of seven) were the Backward2 and Backward1 (visual processing), the 2-back (working memory), and the Stroop4 (stimulus interference) tasks. Thus, we were able to devise cognitive tasks with relatively granular cognitive workload levels. These findings corroborate the internal validity of our cognitive tasks and hint at their ecological one:

- The *2-back task* may represent the complexity of task switching and attention shifting between tasks on an HMD (e.g., responding to a notification), in the real world (e.g., correcting exams), and internal tasks (e.g., trying to recall the exam solutions) (Putze et al., 2016; Vortmann et al., 2019; Vortmann & Putze, 2021).
- The *Backward Masking task(s)* may represent the task of identifying the sought after information or interface element (e.g., finding a skill button when gaming).
- The *Stroop task(s)* could represent situations of conflicting stimuli causing confusion (e.g., choosing from different icons when gaming).

## 6.2. Capturing cognitive workload and inferring cognitive processes

The Alpha band PSD, as captured by the TP9 electrode of *BCIglass*, revealed significant reductions in the Backward2 and Stroop4 tasks, indicating substantial cognitive workload (Grimes et al., 2008; Kosch et al., 2018). Besides, the Alpha band is linked to working memory performance and mental arithmetic tasks (Başar et al., 2001; Klimesch, 1999; Klimesch et al., 1993). We observed no significant Alpha PSD reductions for any *BCIglass* electrode in the 2-back task, as expected during a working memory task (Klimesch, 1999). However, the Nz and TP9 electrodes captured significant fluctuations in the Theta band PSD for the 2-back and Backward1 tasks. In fact, Theta fluctuations are also linked with working memory performance (Klimesch, 1999; Mecklinger et al., 1992), problem-solving and decision-making in oddball paradigms (e.g., Backward1 and Backward2) (Rajan et al., 2019). Interestingly, the *BCIglass* topology captured systematic Theta band PSD fluctuations also for the less cognitively demanding tasks, such as Stroop2 which displayed higher Theta band PSD than the baselines (eyes open & closed)—perhaps an indication of stimulus interference (Hanslmayr et al., 2008). Expectedly, the Delta EEG band displayed the highest number of systematic PSD variations for the top three out of four most cognitively demanding tasks, and for all three *BCIglass* electrodes. These variations were particularly striking when compared with not only the baselines, but also with less cognitively demanding tasks (e.g., Stroop 1, 2 & 3). We believe this is an indication of increased willed attention to internal processing, at least in the Backward1, 2-back, and Stroop4 tasks (Harmony et al., 1996).

Surprisingly, no significant fluctuations were observed both in Delta and Theta PSDs for the Backward2 (masked) task, although displaying substantially high reductions in Alpha band PSD. Prior work has shown that the EEG bands can predict the effectiveness of perceptual masking, and by lowering the intensity of the stimulus, we can reduce the probability of perceiving it to 0 (Schubert et al., 2009). We believe that the stimulus presentation in the Backward2 task was too weak (short) to be perceived (166 ms) by the majority of our participants, as it was subsequently overwritten by the mask presentation (“XXX”). Backward2 task resulted in the lowest average performance score and highest average subjective workload across all cognitive tasks (see Figure 8 and Table 1). Interestingly, we observe that *BCIglass* captured relative Alpha band suppression in the wild too, and in activities that involve visual processing, such as playing a game or watching a movie (Adrian & Matthews, 1934; Jasper, 1936). Notably, the *BCIglass* captured increased relative Beta band when correcting exams, indicating the increased motor preparation and execution for coordinated hand movement (Crone et al., 1998). Capturing naturalistic Beta band fluctuations in the wild is a particularly interesting finding, since no cognitive task that we performed in the lab involved motor preparation and execution (see Section 5.2.4). These findings indicate that even sparse and decentralised EEG-electrode topologies can capture cognitive workload and can infer cognitive processes linked to working memory, decision-making, problem-solving, and internal processing by utilizing the (relative) PSD power of EEG bands—not only in lab settings, but potentially in the wild too (RQ2).

## 6.3. Similar measurements, improved classification accuracy per electrode

Interestingly, we discovered that the higher the Engagement Index (EI), as measured by the Nz and TP10 (*BCIglass*) electrodes, the lower the subjective physical demand (NASA-TLX). The reversed trend was unveiled for the Cz (Enobio 20) electrode, where higher EI displayed a relationship with also higher subjective physical demand. We also found the higher the EI, as measured by the TP9 (*BCIglass*) electrode, the lower the subjective physical demand. These findings are in line with prior literature on the relationship of EI with subjective measures of workload (Kamzanova et al., 2014; Pope et al., 1995), though in a reversed fashion for our prototype. This phenomenon could be attributed to the sparse and decentralized electrode topology of our prototype. In fact, we found that the TP9 and TP10 electrodes (*BCIglass*) measured EI in a similar way to the Cz and Pz (Enobio 20). However, we did not observe the same trend when comparing EI distributions captured by the Nz-Cz and Nz-Pz electrode pairs. We suspect that the Nz (*BCIglass*) electrode was subjected to increased noise interference from face-muscle artifacts. The Nz electrode is placed further away from the Cz and Pz electrodes, right above the nasion (nose) and in close proximity to the procerus and corrugator muscles which produce significant EMG

activity, hindering EEG measurements from that location on the skull. These findings suggest that our experimental *BCIglass* topology captured the compound measure of EI in the same fashion with the Enobio 20, for the selected electrodes (RQ3). Surprisingly, the sparse topology of the *BCIglass* did not seem to drastically affect the classification accuracy of cognitive tasks types, achieving a 79.79% accuracy with a 4-layer CNN model, as opposed to an 88% accuracy for the Enobio 20 with an XGBoost model. This potentially indicates that deep learning approaches, and specifically CNNs, are particularly effective in classifying cognitive tasks based on PSD from scarce electrode topologies (Fridman et al., 2018). Fewer electrodes, placed surreptitiously in contact with the skull, promote the design of lightweight and potentially socially acceptable cognition-aware systems that are fit for everyday-life use.

#### 6.4. Moving EEG into the wild is a prerequisite to cognition-aware systems

Vuzix devices meet the respective electromagnetic compliance (EMC) standards, and thus are suitable for use in healthcare and medical settings. However, due to our covert setup (EEG electrodes attached inside the HMD frame), and the notorious sensitivity of the EEG signals, we still investigated whether any electromagnetic field (EMF) produced by the Vuzix blade can influence the recorded *BCIglass* EEG signals. Measurements with a dedicated EMF meter displayed that only the TP9 electrode was susceptible to high EMF. A deeper look revealed that Vuzix blade produces a notable EMF in the range of 2.4–2.5 GHz (for Wi-Fi connectivity), but far above the usable EEG frequency spectrum to have any effect on it. Even so, a pilot study in the wild enabled us to empirically investigate the EEG signals captured by *BCIglass* when the Vuzix Blade is active. A post-hoc analysis displayed that the *BCIglass* captures EEG activity in the same fashion and irrespective of whether Vuzix Blade is powered on or off. This is an encouraging finding in moving EEG into the wild with *BCIglass*.

*BCIglass* could pave the way for cognition-aware systems, where cognitive workload and cognitive processes are monitored for delivering meaningful and timely interventions (Heger et al., 2010). These interventions could vary from simply selecting the right moment to display an email notification to delivering intrusive warnings when detecting drowsiness during driving (Lin et al., 2008). In fact, the increased connectivity of modern HMDs (BLE, Wi-Fi, 5G) facilitates system interoperability—the communication among different information systems (e.g., (Y. Kim et al., 2015)). In the aforementioned example, the intrusive warning could be delivered via a driver-assistance system that vibrates the steering wheel or disengages cruise control when receiving a command from a *BCIglass* system. By further capitalizing on system interoperability, *BCIglass* could also serve biometric authentication purposes by classifying features extracted from the PSD of EEG bands (Ashby et al., 2011; Zhang et al., 2018) and enabling one to access a personal space (e.g., unlocking a smart-home lock) or system (e.g., online

banking portal). Additional sensors embedded in the frames of a modern HMD could be utilized for developing more sophisticated assistive systems. For example, *BCIglass* could detect moments of low attention in important contexts (e.g., in a meeting) to drive the capture of video via an on-board camera and microphone. The video could later be displayed on the HMD for augmenting memory recall in a “closed-loop” memory-augmentation system.

Despite the recent uptake of mobile in-and around-the ear EEG systems (Ala et al., 2022; Crétot-Richert et al., 2023; Henao et al., 2022; Kaveh et al., 2020; Musaeus et al., 2023), their confined topology in placing EEG electrodes exclusively over the temporal lobe may reduce the quality and the EEG signal they can measure (Kaongoen et al., 2023). Taking into account the proliferation of AR headsets and EEG-powered AR applications (Angrisani et al., 2023; Arpaia et al., 2022; Jang et al., 2023; Zhao et al., 2020), embedding concealed EEG electrodes in lightweight HMDs appears to be a promising avenue. Ultimately, HMDs could be the medium for moving EEG into the wild, while facilitating the design of systems that augment our perceptual and cognitive capacities (Dingler & Niforatos, 2021).

#### 6.5. Limitations

The main part of this study was conducted in a research lab and in stationary settings. We deemed this was necessary to fully determine the feasibility and effectiveness of our concept. Prior work has attempted to introduce EEG in uncontrolled settings involving physical motion (e.g., cycling (Kohli & Casson, 2015) or when driving (Lin et al., 2008)), but so far have utilized an EEG-cap topology by concealing EEG electrodes in helmets (Kohli & Casson, 2015), baseball caps (Lin et al., 2008), or using a typical EEG cap (Casson, 2019). A limited follow-up pilot study in the wild enabled us to explore the real-life potential of *BCIglass* too. In fact, the *BCIglass* was able to capture relative band power in a variety of everyday life activities, displaying a capability we did not recreate in the lab—capturing Beta band power in a motor execution/preparation task. We expect that the on-board sensors of an HMD (e.g., accelerometers) will help us identify opportune moments for EEG sampling in the wild (e.g., when a user is stationary). We also expect that EMG artifacts stemming from muscle contractions may have influenced our results. Although we applied the typical procedures for removing EMG and EOG artifacts, the very position of the Nz electrode between the eyebrow muscles (procerus and corrugator muscles) hinders its capacity to detect EEG activity, when compared with the TP9 and TP10 electrodes. Nevertheless, the Nz electrode was still able to capture significant fluctuations in the Delta and Theta band PSDs linked to cognitive workload and cognitive processes due to effective EEG signal post-processing.

Contrary to popular belief, the prospects of capturing meaningful EEG signals in real-time and on the go are rather positive. For example, the Artifacts Subspace Reconstruction (ASR) algorithm is particularly effective in removing EEG noise artifacts in real time, generated by

muscle contractions and body movement such as facial expressions, speech, walking or even jumping (Kumaravel et al., 2021; Mullen et al., 2015; Tsai et al., 2022). Our first attempt to classify the actual cognitive task at hand was not successful for both systems. Both the *BCIglass* and the Enobio 20 performed poorly when attempting to classify seven (7) different cognitive tasks, with Enobio 20 achieving 8.58% better classification accuracy than *BCIglass*. We attribute this to the scarce data available to effectively train the selected classifier models. Indeed, in a second attempt, we thematically merged the seven different cognitive tasks into three overall cognitive task types. This time, both systems performed substantially better (*BCIglass*: 79.79% | Enobio 20: 88%), with Enobio 20 achieving 8.21% better classification accuracy than *BCIglass*. This stable difference in classification accuracy (~8%) between the two systems, when classifying seven and three cognitive tasks/types, indicates that classification accuracy can be further increased for both systems with more data. Finally, our experimental setup involved the fixation of two EEG systems on the heads of our participants, plus a face mask.<sup>22</sup> As reported, the substantial head-mounted equipment involved, instilled fatigue in our participants. This potentially influenced our results and did not permit longer trials to collect more data. Nevertheless, we could still effectively measure EEG activity owed to the selected cognitive tasks with both systems (*BCIglass* and Enobio 20).

### 6.6. Future work

Our next step is to confirm the ability of the *BCIglass* prototype to capture not only EEG bands but also Event-Related Potentials (ERPs) in longer trials. Previous ERP studies have identified the temporal-parietal sites TP9 and TP10, as two important electrodes in detecting faces through P1, N170, and P2 components (Itier & Taylor, 2002). Thus, we will test whether we can confirm these findings by capturing the ERPs triggered by the perception of faces with our *BCIglass* prototype. ERPs have also been used for obtaining implicit input to systems. For example, Nijholt et al. proposed the use of EEG signals for controlling aspects of game interaction such as triggering special abilities (Nijholt et al., 2009). Thus, ERPs induced by AR overlays, and captured by the *BCIglass*, could serve as a low-cost alternative of eye-gaze interaction with HMDs. We believe the cognitive tasks we devised are ecological enough so as to generate cognitive workload and elicit cognitive processes that manifest in everyday-life settings. In fact, the limited pilot study in the wild unveiled a facet of *BCIglass* we did not investigate in the lab: capturing motor execution/preparation EEG activity. By deploying our 4-layer CNN model on the *BCIglass* prototype and by utilizing the ASR algorithm, we will measure cognitive workload and infer cognitive processes in the wild and in real time, while collecting ground truth via the on-board sensors (e.g., HMD camera). In fact, we can further improve cognitive task classification by applying auto-regressive modelling to predict EEG signal time series (Nai-Jen & Palaniappan, 2004; Wright et al., 1990). Finally, we are also

looking into experimental approaches that utilize deep learning for spatial up-sampling of EEG electrodes, as a remedy for our sparse *BCIglass* topology (Svantesson et al., 2021).

## 7. Conclusion

Open hardware initiatives and the need for ecologically-valid measurements have set sail to democratize EEG by moving it out of the lab and into the users' everyday life. Prior approaches have attempted to conceal EEG electrodes in helmets, caps, earpieces, and some even in a (bulky) pair of sunglasses. In this paper, we showcased how a modern and lightweight Head-Mounted Display (HMD) can be the medium for moving EEG into the wild, in an ergonomic and effective manner. We embedded EEG electrodes into the frame of a Vuzix Blade HMD, at the touchpoints with the skull, creating an covert topology that imposes considerable challenges but also numerous opportunities. We experimentally demonstrated how the *BCIglass* prototype with a limited number of electrodes, situated at the periphery of the human skull, can capture EEG activity in a comparable manner to a higher resolution EEG-cap topology and EEG system (Enobio 20). In fact, the *BCIglass* prototype not only showcases the potential of capturing cognitive workload, but it can also implicitly infer cognitive processes linked to working memory, decision-making, problem-solving, and internal processing in a diverse set of established cognitive tasks. By training a 4-layer CNN, the *BCIglass* topology achieved a better accuracy-over-electrode ratio in classifying cognitive tasks than Enobio 20. A limited pilot study in the wild indicated the potential of the *BCIglass* to capture EEG activity in everyday-life settings too. Ultimately, we posit that *BCIglass* bears the potential to revolutionize a wide range of research and application areas, such as cognition-aware systems, assistive technologies, and human-machine interaction.

## Notes

1. <https://openbci.com/> (Last accessed August 4, 2024).
2. <https://youtu.be/Wpq8S7PKjp4> (EEG artifacts removal with ASR) (Last accessed August 4, 2024).
3. <http://narbis.com/company/> (Last accessed August 4, 2024).
4. <https://solsticesunglasses.com/pages/smithlowdownfocus> (Last accessed August 4, 2024).
5. <https://jins-meme.com/en/> (Last accessed August 4, 2024).
6. <https://looxidlabs.com/product/all> (Last accessed August 4, 2024).
7. <https://neurable.com/> (Last accessed August 4, 2024).
8. <https://www.microsoft.com/en-us/hololens> (Last accessed August 4, 2024).
9. <https://www.vuzix.com/products> (Vuzix, NY, USA) (Last accessed August 4, 2024).
10. <https://shop.openbci.com/collections/frontpage/products/cyton-biosensing-board-8-channel> (OpenBCI, NY, USA) (Last accessed August 4, 2024).
11. <https://webstore.iec.ch/publication/2590> (Last accessed August 4, 2024).
12. [https://www.gqelectronicsllc.com/comersus/store/comersus\\_viewItem.asp?idProduct=5678](https://www.gqelectronicsllc.com/comersus/store/comersus_viewItem.asp?idProduct=5678) (Last accessed August 4, 2024).
13. <https://www.neuroelectrics.com/solutions/enobio/20> (Last accessed August 4, 2024).



14. <https://www.neurobs.com/> (Last accessed August 4, 2024).
15. <https://labstreaminglayer.readthedocs.io/info/intro.html> (Last accessed August 4, 2024).
16. <https://scikit-learn.org/stable/modules/generated/sklearn.svm.SVC.html> (Last accessed August 4, 2024).
17. <https://scikit-learn.org/stable/modules/generated/sklearn.neighbors.KNeighborsClassifier.html> (Last accessed August 4, 2024).
18. <https://www.tensorflow.org/tutorials/images/cnn> (Last accessed August 4, 2024).
19. <https://xgboost.readthedocs.io/en/stable/> (Last accessed August 4, 2024).
20. <https://www.eveonline.com/> (Last accessed August 4, 2024).
21. [https://en.wikipedia.org/wiki/Saving\\_Private\\_Ryan](https://en.wikipedia.org/wiki/Saving_Private_Ryan) (Last accessed August 4, 2024).
22. Mandatory University policy for COVID-19.

## Disclosure statement

No potential conflict of interest was reported by the author(s).

## Funding

The authors acknowledge the financial support of the Swiss National Science Foundation (SNSF) under grant number: 184146. Additionally, the authors acknowledge the financial support of Fundação para a Ciência e Tecnologia (FCT) through the NOISys project [DOI: 10.54499/2022.02283.PTDC].

## ORCID

Evangelos Niforatos  <http://orcid.org/0000-0002-0484-4214>

## References

- Abdelrahman, Y., Velloso, E., Dingler, T., Schmidt, A., & Vetere, F. (2017). Cognitive heat: Exploring the usage of thermal imaging to unobtrusively estimate cognitive load. *Proceedings of the ACM on Interactive, Mobile, Wearable and Ubiquitous Technologies*, 1(3), 1–20. <https://doi.org/10.1145/3130898>
- Adrian, E. D., & Matthews, B. H. (1934). The Berger rhythm: Potential changes from the occipital lobes in man. *Brain*, 57(4), 355–385. <https://doi.org/10.1093/brain/57.4.355>
- Afergan, D., Peck, E. M., Solovey, E. T., Jenkins, A., Hincks, S. W., Brown, E. T., Chang, R., & Jacob, R. J. (2014). Dynamic difficulty using brain metrics of workload. In *Proceedings of the Sigchi Conference on Human Factors in Computing Systems* (pp. 3797–3806). Association for Computing Machinery. <https://doi.org/10.1145/2556288.2557230>
- Ala, T. S., Alickovic, E., Cabrera, A. F., Whitmer, W. M., Hadley, L. V., Rank, M. L., Lunner, T., & Graversen, C. (2022). Alpha oscillations during effortful continuous speech: From scalp EEG to ear-EEG. *IEEE Transactions on Bio-Medical Engineering*, 70(4), 1264–1273. <https://doi.org/10.1109/TBME.2022.3214428>
- Angrisani, L., Arpaia, P., De Benedetto, E., Duraccio, L., Regio, F. L., & Tedesco, A. (2023). Wearable brain-computer interfaces based on steady-state visually evoked potentials and augmented reality: A review. *IEEE Sensors Journal*, 23(15), 16501–16514. <https://doi.org/10.1109/JSEN.2023.3287983>
- Arpaia, P., De Benedetto, E., De Paolis, L., D'Errico, G., Donato, N., & Duraccio, L. (2022). Performance enhancement of wearable instrumentation for AR-based SSVEP BCI. *Measurement*, 196, 111188. <https://doi.org/10.1016/j.measurement.2022.111188>
- Ashby, C., Bhatia, A., Tenore, F., & Vogelstein, J. (2011). Low-cost electroencephalogram (EEG) based authentication. In *2011 5th International IEEE/EMBS Conference on Neural Engineering* (pp. 442–445). IEEE.
- Başar, E., Başar-Eroglu, C., Karakaş, S., & Schürmann, M. (2001). Gamma, alpha, delta, and theta oscillations govern cognitive processes. *International Journal of Psychophysiology: Official Journal of the International Organization of Psychophysiology*, 39(2–3), 241–248. [https://doi.org/10.1016/S0167-8760\(00\)00145-8](https://doi.org/10.1016/S0167-8760(00)00145-8)
- Bernal, G., Yang, T., Jain, A., & Maes, P. (2018). Physiohmd: A conformable, modular toolkit for collecting physiological data from head-mounted displays. In *Proceedings of the 2018 ACM international symposium on wearable computers* (pp. 160–167). Association for Computing Machinery.
- Bleichner, M. G., & Debener, S. (2017). Concealed, unobtrusive ear-centered EEG acquisition: Cee grids for transparent EEG. *Frontiers in Human Neuroscience*, 11, 163. <https://doi.org/10.3389/fnhum.2017.00163>
- Bradley, J. V. (1958). Complete counterbalancing of immediate sequential effects in a Latin square design. *Journal of the American Statistical Association*, 53(282), 525–528. <https://doi.org/10.1080/01621459.1958.10501456>
- Buzsáki, G., & Draguhn, A. (2004). Neuronal oscillations in cortical networks. *Science (New York, N.Y.)*, 304(5679), 1926–1929. <https://doi.org/10.1126/science.1099745>
- Casson, A. J. (2019). Wearable EEG and beyond. *Biomedical Engineering Letters*, 9(1), 53–71. <https://doi.org/10.1007/s13534-018-00093-6>
- Chwalek, P., Ramsay, D., & Paradiso, J. A. (2021). Captivates: A smart eyeglass platform for across-context physiological measurement. *Proceedings of the ACM on Interactive, Mobile, Wearable and Ubiquitous Technologies*, 5(3), 1–32. <https://doi.org/10.1145/3478079>
- Crétoir-Richert, G., De Vos, M., Debener, S., Bleichner, M. G., & Voix, J. (2023). Assessing focus through ear-EEG: A comparative study between conventional cap EEG and mobile in-and around-the-ear eeg systems. *Frontiers in Neuroscience*, 17, 895094. <https://doi.org/10.3389/fnins.2023.895094>
- Crone, N. E., Miglioretti, D. L., Gordon, B., & Lesser, R. P. (1998). Functional mapping of human sensorimotor cortex with electrocorticographic spectral analysis. II. Event-related synchronization in the gamma band. *Brain: a Journal of Neurology*, 121 (Pt 12), 2301–2315. <https://doi.org/10.1093/brain/121.12.2301>
- Cutrell, E., & Tan, D. (2008, April). BCI for passive input in HCI. In *Proceedings of CHI* (Vol. 8, pp. 1–3). ACM Press.
- Davis, C. E., Hauf, J. D., Wu, D. Q., & Everhart, D. E. (2011). Brain function with complex decision making using electroencephalography. *International Journal of Psychophysiology: Official Journal of the International Organization of Psychophysiology*, 79(2), 175–183. <https://doi.org/10.1016/j.ijpsycho.2010.10.004>
- Delorme, A., & Makeig, S. (2004). Eeglab: An open source toolbox for analysis of single-trial EEG dynamics including independent component analysis. *Journal of Neuroscience Methods*, 134(1), 9–21. <https://doi.org/10.1016/j.jneumeth.2003.10.009>
- Dingler, T., & Niforatos, E. (2021). *Technology-augmented perception and cognition* (1st ed.). Springer.
- Fang, L., Xing, S. P., Ma, Z., Zhang, Z., Long, Y., Lee, K.-P., & Wang, S. J. (2023). EMO-mg framework: LSTM-based multi-modal emotion detection through electroencephalography signals and micro gestures. *International Journal of Human-Computer Interaction*. Advance online publication. <https://doi.org/10.1080/10447318.2023.2228983>
- Fedosov, A., Niforatos, E., Elhart, I., Schneider, T., Anisimov, D., & Langheinrich, M. (2016). Design and evaluation of a wearable ar system for sharing personalized content on SKI resort maps. In *Proceedings of the 15th International Conference on Mobile and Ubiquitous Multimedia* (pp. 141–152). Association for Computing Machinery. <https://doi.org/10.1145/3012709.3012721>
- Fridman, L., Reimer, B., Mehler, B., & Freeman, W. T. (2018). Cognitive load estimation in the wild. In *Proceedings of the 2018 Chi Conference on Human Factors in Computing Systems* (pp. 1–9). Association for Computing Machinery. <https://doi.org/10.1145/3173574.3174226>



- Ghiani, G., Manca, M., & Paternò, F. (2015). Dynamic user interface adaptation driven by physiological parameters to support learning. In *Proceedings of the 7th ACM Sigchi Symposium on Engineering Interactive Computing Systems* (pp. 158–163). Association for Computing Machinery. <https://doi.org/10.1145/2774225.2775081>
- Grimes, D., Tan, D. S., Hudson, S. E., Shenoy, P., & Rao, R. P. (2008). Feasibility and pragmatics of classifying working memory load with an electroencephalograph. In *Proceedings of the Sigchi Conference on Human Factors in Computing Systems* (pp. 835–844). Association for Computing Machinery. <https://doi.org/10.1145/1357054.1357187>
- Gugenheimer, J., Mai, C., McGill, M., Williamson, J., Steinicke, F., & Perlin, K. (2019). Challenges using head-mounted displays in shared and social spaces. In *Extended Abstracts of the 2019 Chi Conference on Human Factors in Computing Systems* (pp. 1–8). Association for Computing Machinery. <https://doi.org/10.1145/3290607.3299028>
- Hanslmayr, S., Pastötter, B., Bäuml, K.-H., Gruber, S., Wimber, M., & Klimesch, W. (2008). The electrophysiological dynamics of interference during the stroop task. *Journal of Cognitive Neuroscience*, 20(2), 215–225. <https://doi.org/10.1162/jocn.2008.20020>
- Harmony, T., Fernández, T., Silva, J., Bernal, J., Díaz-Comas, L., Reyes, A., Marosi, E., Rodríguez, M., & Rodríguez, M. (1996). EEG delta activity: An indicator of attention to internal processing during performance of mental tasks. *International Journal of Psychophysiology: Official Journal of the International Organization of Psychophysiology*, 24(1-2), 161–171. [https://doi.org/10.1016/s0167-8760\(96\)00053-0](https://doi.org/10.1016/s0167-8760(96)00053-0)
- Hart, S. G., & Staveland, L. E. (1988). Development of nasa-tlx (task load index): Results of empirical and theoretical research. In *Advances in psychology* (Vol. 52, pp. 139–183). Elsevier.
- Heger, D., Putze, F., & Schultz, T. (2010). Online workload recognition from eeg data during cognitive tests and human-machine interaction. In *Annual Conference on Artificial Intelligence* (pp. 410–417). Springer.
- Henao, D., Navarrete, M., Juez, J. Y., Dinh, H., Gómez, R., Valderrama, M., & Le Van Quyen, M. (2022). Auditory closed-loop stimulation on sleep slow oscillations using in-ear EEG sensors. *Journal of Sleep Research*, 31(6), e13555. <https://doi.org/10.1111/jsr.13555>
- Huang, J., Yu, C., Wang, Y., Zhao, Y., Liu, S., Mo, C., Liu, J., Zhang, L., & Shi, Y. (2014). Focus: Enhancing children's engagement in reading by using contextual BCI training sessions. In *Proceedings of the sigchi conference on human factors in computing systems* (pp. 1905–1908). Association for Computing Machinery.
- Itier, R. J., & Taylor, M. J. (2002). Inversion and contrast polarity reversal affect both encoding and recognition processes of unfamiliar faces: A repetition study using erps. *NeuroImage*, 15(2), 353–372. <https://doi.org/10.1006/nimg.2001.0982>
- Jaeggi, S. M., Buschkuhl, M., Perrig, W. J., & Meier, B. (2010). The concurrent validity of the n-back task as a working memory measure. *Memory (Hove, England)*, 18(4), 394–412. <https://doi.org/10.1080/09658211003702171>
- Jang, H., Park, S., Woo, J., Ha, J., & Kim, L. (2023). Authentication system based on event-related potentials using AR glasses. In *2023 11th International Winter Conference on Brain-Computer Interface (BCI)* (pp. 1–4). IEEE. <https://doi.org/10.1109/BCI57258.2023.10078487>
- Jantz, J., Molnar, A., & Alcaide, R. (2017). A brain-computer interface for extended reality interfaces. In *ACM Siggraph 2017 VR Village* (pp. 1–2). ACM. <https://doi.org/10.1145/3089269.3089290>
- Jasper, H. H. (1936). Cortical excitatory state and variability in human brain rhythms. *Science (New York, N.Y.)*, 83(2150), 259–260. <https://doi.org/10.1126/science.83.2150.259>
- Jurewicz, K., Paluch, K., Kublik, E., Rogala, J., Mikicin, M., & Wróbel, A. (2018). EEG-neurofeedback training of beta band (12–22 Hz) affects alpha and beta frequencies—a controlled study of a healthy population. *Neuropsychologia*, 108, 13–24. <https://doi.org/10.1016/j.neuropsychologia.2017.11.021>
- Kabe, A. M., & Sako, B. H. (2020). Chapter 5 - analysis of continuous and discrete time signals. In A. M. Kabe & B. H. Sako (Eds.), *Structural dynamics fundamentals and advanced applications* (pp. 271–427). Academic Press. <https://www.sciencedirect.com/science/article/pii/B9780128216156000058>
- Kamzanova, A. T., Kustubayeva, A. M., & Matthews, G. (2014). Use of EEG workload indices for diagnostic monitoring of vigilance decrement. *Human Factors*, 56(6), 1136–1149. <https://doi.org/10.1177/0018720814526617>
- Kane, M. J., Conway, A. R., Miura, T. K., & Colflesh, G. J. (2007). Working memory, attention control, and the n-back task: A question of construct validity. *Journal of Experimental Psychology: Learning, Memory, and Cognition*, 33(3), 615–622. <https://doi.org/10.1037/0278-7393.33.3.615>
- Kaongoen, N., Choi, J., Woo Choi, J., Kwon, H., Hwang, C., Hwang, G., Kim, B. H., & Jo, S. (2023). The future of wearable EEG: A review of ear-EEG technology and its applications. *Journal of Neural Engineering*, 20(5), 051002. <https://doi.org/10.1088/1741-2552/acfdca>
- Kar, P., & Hazarika, J. (2023). An efficacy analysis of affect representation methodologies used in EEG-based emotion recognition system: An unsupervised approach. *International Journal of Human-Computer Interaction*. Advance online publication. <https://doi.org/10.1080/10447318.2023.2254626>
- Katona, J., Ujbanyi, T., Sziladi, G., & Kovari, A. (2016). Speed control of festo robotino mobile robot using neurosky mindwave EEG headset based brain-computer interface. In *2016 7th IEEE International Conference on Cognitive Infocommunications (CogInfoCom)* (pp. 251–256). IEEE. <https://doi.org/10.1109/CogInfoCom.2016.7804557>
- Kaveh, R., Doong, J., Zhou, A., Schwendeman, C., Gopalan, K., Burghardt, F. L., Arias, A. C., Maharbiz, M. M., & Muller, R. (2020). Wireless user-generic ear EEG. *IEEE Transactions on Biomedical Circuits and Systems*, 14(4), 727–737. <https://doi.org/10.1109/TBCAS.2020.3001265>
- Kim, S., & Dey, A. K. (2009). Simulated augmented reality windshield display as a cognitive mapping aid for elder driver navigation. In *Proceedings of the Sigchi Conference on Human Factors in Computing Systems* (pp. 133–142). Association for Computing Machinery. <https://doi.org/10.1145/1518701.1518724>
- Kim, Y., Kaongoen, N., & Jo, S. (2015). Hybrid-BCI smart glasses for controlling electrical devices. In *2015 54th Annual Conference of the Society of Instrument and Control Engineers of Japan (SICE)* (pp. 1162–1166). IEEE. <https://doi.org/10.1109/SICE.2015.7285345>
- Klimesch, W. (1999). Eeg alpha and theta oscillations reflect cognitive and memory performance: A review and analysis. *Brain Research Reviews*, 29(2-3), 169–195. [https://doi.org/10.1016/s0165-0173\(98\)00056-3](https://doi.org/10.1016/s0165-0173(98)00056-3)
- Klimesch, W., Schimke, H., & Pfurtscheller, G. (1993). Alpha frequency, cognitive load and memory performance. *Brain Topography*, 5(3), 241–251. <https://doi.org/10.1007/BF01128991>
- Koelle, M., Kranz, M., & Möller, A. (2015). Don't look at me that way!: Understanding user attitudes towards data glasses usage. In *Proceedings of the 17th International Conference on Human-Computer Interaction with Mobile Devices and Services* (pp. 362–372). Association for Computing Machinery. <https://dl.acm.org/doi/10.1145/2785830.2785842>
- Kohli, S., & Casson, A. J. (2015). Towards out-of-the-lab EEG in uncontrolled environments: Feasibility study of dry EEG recordings during exercise bike riding. In *2015 37th Annual International Conference of the IEEE Engineering in Medicine and Biology Society (EMBC)* (pp. 1025–1028). IEEE. <https://doi.org/10.1109/EMBC.2015.7318539>
- Kosch, T., Funk, M., Schmidt, A., & Chuang, L. L. (2018). Identifying cognitive assistance with mobile electroencephalography: A case study with in-situ projections for manual assembly. *Proceedings of the ACM on Human-Computer Interaction*, 2(EICS), 1–20. <https://doi.org/10.1145/3229093>
- Kosch, T., Schmidt, A., Thanheiser, S., & Chuang, L. L. (2020). One does not simply RSVP: Mental workload to select speed reading parameters using electroencephalography. In *Proceedings of the 2020 Sigchi Conference on Human Factors in Computing Systems* (pp. 1–13). Association for Computing Machinery.
- Krigolson, O. E., Williams, C. C., Norton, A., Hassall, C. D., & Colino, F. L. (2017). Choosing muse: Validation of a low-cost, portable EEG system for ERP research. *Frontiers in Neuroscience*, 11, 109. <https://doi.org/10.3389/fnins.2017.00109>
- Kühn, S., Romanowski, A., Schilling, C., Lorenz, R., Mörsen, C., Seiferth, N., Banaschewski, T., Barbot, A., Barker, G. J., Büchel, C., Conrad, P. J., Dalley, J. W., Flor, H., Garavan, H., Ittermann, B., Mann, K., Martinot, J.-L., Paus, T., Rietschel, M., ... Gallinat, J.

- (2011). The neural basis of video gaming. *Translational Psychiatry*, 1(11), e53. <https://doi.org/10.1038/tp.2011.53>
- Kumaravel, V. P., Kartsch, V., Benatti, S., Vallortigara, G., Farella, E., & Buiatti, M. (2021). Efficient artifact removal from low-density wearable EEG using artifacts subspace reconstruction. In *2021 43rd annual international conference of the IEEE engineering in medicine & biology society (EMBC)* (pp. 333–336). <https://doi.org/10.1109/EMBC46164.2021.9629771>
- Lee, Y.-C., Lin, W.-C., King, J.-T., Ko, L.-W., Huang, Y.-T., & Cherng, F.-Y. (2014). An eeg-based approach for evaluating audio notifications under ambient sounds. In *Proceedings of the Sigchi Conference on Human Factors in Computing Machinery* (pp. 3817–3826). Association for Computing Machinery. <https://doi.org/10.1145/2556288.2557076>
- Lin, C.-T., Chen, Y.-C., Huang, T.-Y., Chiu, T.-T., Ko, L.-W., Liang, S.-F., Hsieh, H.-Y., Hsu, S.-H., & Duann, J.-R. (2008). Development of wireless brain computer interface with embedded multitask scheduling and its application on real-time driver's drowsiness detection and warning. *IEEE Transactions on Bio-Medical Engineering*, 55(5), 1582–1591. <https://doi.org/10.1109/TBME.2008.918566>
- Lotte, F., Bougrain, L., Cichocki, A., Clerc, M., Congedo, M., Rakotomamonjy, A., & Yger, F. (2018). A review of classification algorithms for EEG-based brain–computer interfaces: A 10 year update. *Journal of Neural Engineering*, 15(3), 031005. <https://doi.org/10.1088/1741-2552/aab2f2>
- Mai, C., Hassib, M., & Königbauer, R. (2017). Estimating visual discomfort in head-mounted displays using electroencephalography. In *IFIP Conference on Human-Computer Interaction* (pp. 243–252). Springer International Publishing.
- Makeig, S., Jung, T.-P., Ghahremani, D., & Sejnowski, T. J. (1996). Independent component analysis of simulated erp data. *Institute for Neural Computation, University of California: technical report INC-9606*.
- Mecklinger, A., Kramer, A. F., & Strayer, D. L. (1992). Event related potentials and EEG components in a semantic memory search task. *Psychophysiology*, 29(1), 104–119. <https://doi.org/10.1111/j.1469-8986.1992.tb02021.x>
- Messerotti Benvenuti, S., Mennella, R., Buodo, G., & Palomba, D. (2017). Frontal theta activity as an EEG correlate of mood-related emotional processing in dysphoria. *Journal of Psychopathology and Behavioral Assessment*, 39(2), 241–252. <https://doi.org/10.1007/s10862-016-9572-8>
- Moisala, M., Salmela, V., Hietajärvi, L., Carlson, S., Vuontela, V., Lonka, K., Hakkarainen, K., Salmela-Aro, K., & Alho, K. (2017). Gaming is related to enhanced working memory performance and task-related cortical activity. *Brain Research*, 1655, 204–215. <https://doi.org/10.1016/j.brainres.2016.10.027>
- Mondellini, M., Pirovano, I., Colombo, V., Arlati, S., Sacco, M., Rizzo, G., & Mastropietro, A. (2023). A multimodal approach exploiting EEG to investigate the effects of VR environment on mental workload. *International Journal of Human-Computer Interaction*. Advance online publication. <https://doi.org/10.1080/10447318.2023.2258017>
- Mullen, T. R., Kothe, C. A. E., Chi, Y. M., Ojeda, A., Kerth, T., Makeig, S., Jung, T.-P., & Cauwenberghs, G. (2015). Real-time neuroimaging and cognitive monitoring using wearable dry EEG. *IEEE Transactions on Bio-Medical Engineering*, 62(11), 2553–2567. <https://doi.org/10.1109/TBME.2015.2481482>
- Musaeus, C. S., Frederiksen, K. S., Andersen, B. B., Høgh, P., Kidmose, P., Fabricius, M., Hribljan, M. C., Hemmsen, M. C., Rank, M. L., Waldemar, G., & Kjær, T. W. (2023). Detection of subclinical epileptiform discharges in Alzheimer's disease using long-term outpatient EEG monitoring. *Neurobiology of Disease*, 183, 106149. <https://doi.org/10.1016/j.nbd.2023.106149>
- Nacke, L. E., Kalyn, M., Lough, C., & Mandryk, R. L. (2011). Biofeedback game design: Using direct and indirect physiological control to enhance game interaction. In *Proceedings of the SIGCHI conference on human factors in computing systems* (pp. 103–112). Association for Computing Machinery.
- Nai-Jen, H., & Palaniappan, R. (2004). Classification of mental tasks using fixed and adaptive autoregressive models of EEG signals. In *The 26th annual international conference of the IEEE engineering in medicine and biology society* (Vol. 1, p. 507–510). IEEE. <https://doi.org/10.1109/IEMBS.2004.1403205>
- Narsimha Reddy, C., Mahesh, S., & Manjunathachari, K. (2023). Hybrid feature integration model and adaptive transformer approach for emotion recognition with EEG signals. *Computer Methods in Biomechanics and Biomedical Engineering*. Advance online publication. <https://doi.org/10.1080/10255842.2023.2252551>
- Newson, J. J., & Thiagarajan, T. C. (2018). EEG frequency bands in psychiatric disorders: A review of resting state studies. *Frontiers in Human Neuroscience*, 12, 521. <https://doi.org/10.3389/fnhum.2018.00521>
- Nie, D., Wang, X.-W., Shi, L.-C., & Lu, B.-L. (2011). EEG-based emotion recognition during watching movies. In *2011 5th International IEEE/EMBS Conference on Neural Engineering* (pp. 667–670). IEEE.
- Nijholt, A., Bos, D. P.-O., & Reuderink, B. (2009). Turning shortcomings into challenges: Brain–computer interfaces for games. *Entertainment Computing*, 1(2), 85–94. <https://doi.org/10.1016/j.entcom.2009.09.007>
- Pereira, D. G., Afonso, A., & Medeiros, F. M. (2015). Overview of Friedman's test and post-hoc analysis. *Communications in Statistics - Simulation and Computation*, 44(10), 2636–2653. <https://doi.org/10.1080/03610918.2014.931971>
- Pion-Tonachini, L., Makeig, S., & Kreutz-Delgado, K. (2017). Crowd labeling latent dirichlet allocation. *Knowledge and Information Systems*, 53(3), 749–765. <https://doi.org/10.1007/s10115-017-1053-1>
- Pope, A. T., Bogart, E. H., & Bartolome, D. S. (1995). Biocybernetic system evaluates indices of operator engagement in automated task. *Biological Psychology*, 40(1–2), 187–195. [https://doi.org/10.1016/0301-0511\(95\)05116-3](https://doi.org/10.1016/0301-0511(95)05116-3)
- Putze, F., Scherer, M., & Schultz, T. (2016). Starring into the void? Classifying internal vs. external attention from EEG. In *Proceedings of the 9th Nordic Conference on Human-Computer Interaction* (pp. 1–4). Association for Computing Machinery.
- Rajan, A., Siegel, S. N., Liu, Y., Bengson, J., Mangun, G. R., & Ding, M. (2019). Theta oscillations index frontal decision-making and mediate reciprocal frontal–parietal interactions in willed attention. *Cerebral Cortex* (New York, N.Y.: 1991), 29(7), 2832–2843. <https://doi.org/10.1093/cercor/bhy149>
- Rehman, U., & Cao, S. (2016). Augmented-reality-based indoor navigation: A comparative analysis of handheld devices versus google glass. *IEEE Transactions on Human-Machine Systems*, 47(1), 1–12. <https://doi.org/10.1109/THMS.2016.2620106>
- Rypma, B., & D'Esposito, M. (1999). The roles of prefrontal brain regions in components of working memory: Effects of memory load and individual differences. *Proceedings of the National Academy of Sciences of the United States of America*, 96(11), 6558–6563. <https://doi.org/10.1073/pnas.96.11.6558>
- Schneegass, C., Kosch, T., Baumann, A., Rusu, M., Hassib, M., & Hussmann, H. (2020). Braincode: Electroencephalography-based comprehension detection during reading and listening. In *Proceedings of the 2020 SIGCHI conference on human factors in computing systems* (pp. 1–13). Association for Computing Machinery.
- Schubert, R., Haufe, S., Blankenburg, F., Villringer, A., & Curio, G. (2009). Now you'll feel it, now you won't: EEG rhythms predict the effectiveness of perceptual masking. *Journal of Cognitive Neuroscience*, 21(12), 2407–2419. <https://doi.org/10.1162/jocn.2008.21174>
- Setz, C., Arnrich, B., Schumm, J., La Marca, R., Tröster, G., & Ehlert, U. (2009). Discriminating stress from cognitive load using a wearable EDA device. *IEEE Transactions on Information Technology in Biomedicine: a Publication of the IEEE Engineering in Medicine and Biology Society*, 14(2), 410–417. <https://doi.org/10.1109/TITB.2009.2036164>
- Siegel, S. (1956). *Nonparametric statistics for the behavioral sciences*. McGraw-Hill.
- Simmons, A. M., & Luck, S. J. (2020). Protocol for reducing COVID-19 transmission risk in EEG research. *Research Square* [Preprint]. 2020 Jul 22:rs.3.pex-974. <https://doi.org/10.21203/rs.3.pex-974/v2>
- Sopic, D., Aminifar, A., & Atienza, D. (2018). e-glass: A wearable system for real-time detection of epileptic seizures. In *2018 IEEE International Symposium on Circuits and Systems (ISCAS)* (pp. 1–5). IEEE. <https://doi.org/10.1109/ISCAS.2018.8351728>

- Svantesson, M., Olausson, H., Eklund, A., & Thordstein, M. (2021). Virtual EEG-electrodes: Convolutional neural networks as a method for upsampling or restoring channels. *Journal of Neuroscience Methods*, 355, 109126. <https://doi.org/10.1016/j.jneumeth.2021.109126>
- Szafir, D., & Mutlu, B. (2012). Pay attention! Designing adaptive agents that monitor and improve user engagement. In *Proceedings of the sigchi conference on human factors in computing systems* (pp. 11–20). Association for Computing Machinery.
- Tang, A., Owen, C., Biocca, F., & Mou, W. (2003). Comparative effectiveness of augmented reality in object assembly. In *Proceedings of the Sigchi Conference on Human Factors in Computing Systems* (pp. 73–80). Association for Computing Machinery. <https://doi.org/10.1145/642611.642626>
- Tsai, B.-Y., Diddi, S. V. S., Ko, L.-W., Wang, S.-J., Chang, C.-Y., & Jung, T.-P. (2022). Development of an adaptive artifact subspace reconstruction based on hebbian/anti-hebbian learning networks for enhancing BCI performance. *IEEE Transactions on Neural Networks and Learning Systems*, 35(1), 348–361. <https://doi.org/10.1109/TNNLS.2022.3174528>
- Uema, Y., & Inoue, K. (2017). Jins meme algorithm for estimation and tracking of concentration of users. In *Proceedings of the 2017 ACM International Joint Conference on Pervasive and Ubiquitous Computing and Proceedings of the 2017 ACM International Symposium on Wearable Computers* (pp. 297–300). Association for Computing Machinery.
- Verney, S. P., Granholm, E., & Marshall, S. P. (2004). Pupillary responses on the visual backward masking task reflect general cognitive ability. *International Journal of Psychophysiology: official Journal of the International Organization of Psychophysiology*, 52(1), 23–36. <https://doi.org/10.1016/j.ijpsycho.2003.12.003>
- Vi, C., & Subramanian, S. (2012). Detecting error-related negativity for interaction design. In *Proceedings of the Sigchi Conference on Human Factors in Computing Systems* (pp. 493–502). Association for Computing Machinery. <https://doi.org/10.1145/2207676.2207744>
- Vortmann, L.-M., & Putze, F. (2021). Exploration of person-independent bcis for internal and external attention-detection in augmented reality. *Proceedings of the ACM on Interactive, Mobile, Wearable and Ubiquitous Technologies*, 5(2), 1–27. <https://doi.org/10.1145/3463507>
- Vortmann, L.-M., Schult, M., Benedek, M., Walcher, S., & Putze, F. (2019). Real-time multimodal classification of internal and external attention. In *Adjunct of the 2019 International Conference on Multimodal Interaction* (pp. 1–7). Association for Computing Machinery. <https://doi.org/10.1145/3351529.3360658>
- Vourvopoulos, A., & Bermudez I Badia, S. (2016). Usability and cost-effectiveness in brain-computer interaction: Is it user throughput or technology related? In *Proceedings of the 7th Augmented Human International Conference 2016* (p. 19). Association for Computing Machinery.
- Vourvopoulos, A., Niforatos, E., & Giannakos, M. (2019). Eeglass: An eeg-eyeware prototype for ubiquitous brain-computer interaction. In *Adjunct Proceedings of the 2019 ACM International Joint Conference on Pervasive and Ubiquitous Computing and Proceedings of the 2019 ACM International Symposium on Wearable Computers* (pp. 647–652). Association for Computing Machinery.
- Welch, P. (1967). The use of fast Fourier transform for the estimation of power spectra: A method based on time averaging over short, modified periodograms. *IEEE Transactions on Audio and Electroacoustics*, 15(2), 70–73. <https://doi.org/10.1109/TAU.1967.1161901>
- Wright, J., Kydd, R., & Sergejew, A. (1990). Autoregression models of EEG. *Biological Cybernetics*, 62(3), 201–210. <https://doi.org/10.1007/BF00198095>
- Young, M. S., Brookhuis, K. A., Wickens, C. D., & Hancock, P. A. (2015). State of science: Mental workload in ergonomics. *Ergonomics*, 58(1), 1–17. <https://doi.org/10.1080/00140139.2014.956151>
- Zhang, X., Yao, L., Kanhere, S. S., Liu, Y., Gu, T., & Chen, K. (2018). Mindid: Person identification from brain waves through attention-based recurrent neural network. *Proceedings of the ACM on Interactive, Mobile, Wearable and Ubiquitous Technologies*, 2(3), 1–23. <https://doi.org/10.1145/3264959>
- Zhao, X., Liu, C., Xu, Z., Zhang, L., & Zhang, R. (2020). SSVEP stimulus layout effect on accuracy of brain-computer interfaces in augmented reality glasses. *IEEE Access*, 8, 5990–5998. <https://doi.org/10.1109/ACCESS.2019.2963442>
- Zoefel, B., Huster, R. J., & Herrmann, C. S. (2011). Neurofeedback training of the upper alpha frequency band in eeg improves cognitive performance. *NeuroImage*, 54(2), 1427–1431. <https://doi.org/10.1016/j.neuroimage.2010.08.078>

## About the authors

**Evangelos Niforatos** is Assistant Professor on AI-Powered Human Augmentation at the Faculty of Industrial Design Engineering, TU Delft. His research focuses on designing and developing AI systems that augment human perception and cognition. Ultimately, he is interested in utilising technology for extending human abilities beyond the humanly possible.

**Tianhao He** is a Ph.D. candidate at the Faculty of Industrial Design Engineering in TU Delft. As a member of the Design-at-Scale Lab, he is dedicated to Designer-AI Collaboration. His research spans Generative AI and Computer Vision, aiming to develop applied tools for professional uses.

**Athanasios Vourvopoulos** is Assistant Professor in the Bioengineering Department of IST/University of Lisbon, and Principal Investigator at the Institute for Systems and Robotics (ISR-Lisboa). Primary research focuses on non-invasive neural interfacing with virtual environments and robotic systems for restoration, augmentation, and control for individuals suffering from neurological or cardiovascular disorders.

**Michail Giannakos** is Professor in interaction design and learning technology with the Department of Computer Science and leads the Learner-Computer Interaction Lab at the Norwegian University of Science and Technology (NTNU), Trondheim, Norway. His research interests center on developing new ways for humans to interact with interactive learning systems.